Article

Non-Covalent Protein Arginine Deiminase (PAD) Inhibitors Are Efficacious in Animal Models of Multiple Sclerosis

Elizabeth J. Curiel Tejeda, Angelica M Bello, Ewa Wasilewski, Adam Koebel, Shannon Dunn, and Lakshmi P Kotra

J. Med. Chem., **Just Accepted Manuscript** • DOI: 10.1021/acs.jmedchem.7b01102 • Publication Date (Web): 18 Oct 2017

Non-Covalent Protein Arginine Deiminase (PAD) Inhibitors Are Efficacious in Animal Models of Multiple Sclerosis

*Elizabeth J. Curiel Tejeda,[1] Angelica M. Bello,[1,2] Ewa Wasilewski[1,2], Adam Koebel,[1,2] Shannon Dunn,[2,3] and Lakshmi P. Kotra[1,2,4]**

[1]Department of Pharmaceutical Sciences, Leslie Dan Faculty of Pharmacy, University of Toronto, Ontario, Canada, M5S 3M2

[2]Centre for Molecular Design and Preformulations, Toronto General Hospital Research Institute, University Health Network, Toronto, Ontario, Canada, M5G 1L7

[3]Department of Immunology, University of Toronto, Medical Sciences Building, 1 King's College Circle, Toronto, Ontario, Canada M5S 1A8

[4]Multi-Organ Transplant Program, Toronto General Hospital, 200, Elizabeth Street, Toronto, Ontario, Canada, M5G 2C4

KEYWORDS: Protein arginine deiminases, multiple sclerosis, non-covalent inhibitors, EAE, L-homoserine.

RECEIVED DATE (to be automatically inserted)

Abstract.

Peptidyl arginine deiminases have been shown to be hyperactive in neurodegenerative diseases including multiple sclerosis. An α-amino acid based core structure, derived from a hydantoin core, with unique heterocycles on the side chains were synthesized as potential non-covalent inhibitors of PAD enzymes. Amongst the various heterocycles investigated, compound **23** carrying an imidazole moiety, exhibited the highest potency in this series with some selectivity for PAD2, and was further investigated *in vivo*. Pharmacokinetics in mice suggested the C_{max} to be 12.0 ± 2.5 μg/mL and 170 ± 10 ng/mL in the serum and brain, respectively, when compound **23** was administered at 50 mg/kg via single dose *i.p.* At the same dose, compound **23** also reversed physical disability and cleared the brain of T-cell infiltration in an EAE mouse model of multiple sclerosis (MS). This novel series of compounds show promise for further development as disease modifying agents for the potential treatment of MS.

Introduction.

Citrullination is a post-translational modification that consists of the deimination of peptidyl arginine residues into peptidyl citrulline (Scheme 1), and is known to play an essential role in physiological processes such as skin keratinization, insulation of neuronal axons, gene regulation, and maintenance of plasticity of the central nervous system (CNS).[1,2] Citrullination is a process mainly regulated by the Ca^{2+}-dependent amidinotransferase family of enzymes known as protein arginine deiminases (PADs).[3] Five PAD isozymes in humans, PAD 1-4 and PAD6, with well-conserved primary structure exhibit tissue-specific expression patterns.[3] The deregulation of this posttranslational modification has been associated with neurodegenerative and immunopathological conditions such as rheumatoid arthritis (RA),[4] Alzheimer's disease (AD),[5] and multiple sclerosis (MS).[6,7,8,9]

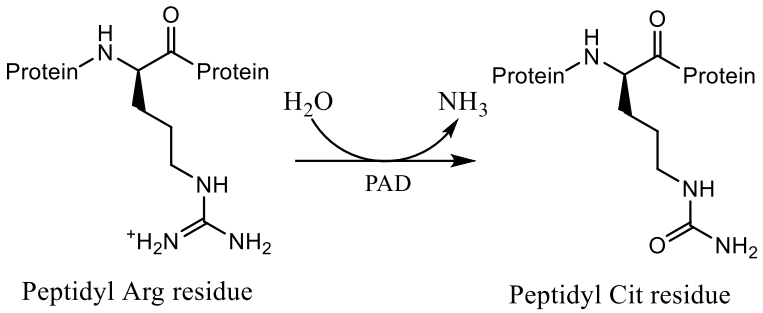

Peptidyl Arg residue Peptidyl Cit residue

Scheme 1. Citrullination (deimination) of peptidyl Arg residue by PAD enzymes.

Due to their potential role in disease pathogenesis, the development of inhibitors towards PADs for therapeutic use has become of high importance. In the past decade, a series of known drugs were evaluated and compounds such as taxol, streptomycin, and several tetracycline derivatives have shown reversible inhibitory properties towards PAD enzymes, albeit with relatively poor potency and selectivity.[10,11] To date a number of PAD inhibitors, primarily covalent modifiers, were identified which contain a terminal haloacetamidine warhead.[12-22] These inhibitors have been observed as good modulators of NET trap formation, transcriptional regulation in cancer, and remyelination in MS animal models.[12,23] Despite their high potency, concerns remain regarding potential nonspecific

reactivity of these electrophilic covalent modifiers and their suitability as potential drugs.

PAD enzymes and their inhibitors have been studied in relation to myelin modification, relevant to MS as well as the myelin oligodendrocyte glycoprotein induced experimental autoimmune encephalomyelitis (MOG-EAE) in mice.[23,24,25,26] This is routinely used acute EAE model for MS, which is a CD4(+) T cell-driven model, induced with the immunodominant 35-55 peptide of myelin oligodendrocyte glycoprotein ($pMOG_{35-55}$) and was used to test whether citrullination of a T cell epitope can contribute to disease etiopathology.[27,28] PAD2 and PAD4 enzymes are significantly upregulated in the inflamed CNS in this animal model. T cells that responded specifically to the citrullinated pMOG could not initiate the EAE lesion, but these cells could provoke exacerbation of pathology if transferred into mice with an ongoing EAE. A similar study using the peptides from myelin basic protein (MBP) epitopes indicated that self-antigens could potentially trigger the disease in susceptible individuals carrying citrullinated peptide epitopes.[29,30] It is also noted that citrulline is more frequently identified in the brains of patients with early onset MS than in healthy subjects using magnetic resonance spectroscopy.[31] This study and others have established the direct correlation between hypercitrullination and disease progression in MS.[32]

Our group took an *in silico* approach to identify non-covalent inhibitors by exploiting cationic, anionic, and hydrophobic binding interactions within the active site pocket of PAD4 enzyme.[33] From this library of inhibitors, a hydantoin derivative **1** (Figure 1) showed key binding interactions between the active site residues Asp350, Asp473, and the piperazine moiety, as well as hydrogen bonding between the hydantoin moiety and the surface Arg374 residue that stabilized binding interactions and potentially led to higher potency (K_i = 131 μM).

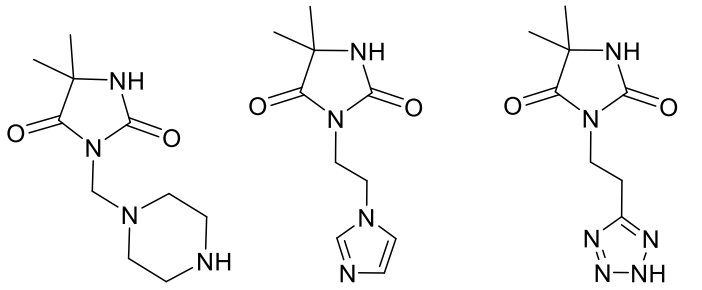

Figure 1. Hydantoin series of non-covalent PAD inhibitors.

Recently, we published a structure-activity relationship investigation that evaluated the activity of further hydantoin derivatives tethered via a two-carbon, instead of single carbon, linker with a variety of nitrogen-rich heterocycles.[34] Interestingly, increasing the linker length was sufficient to reduce the binding affinity of piperazinyl derivatives. Instead, compounds **2** and **3** with 5-membered heterocycles were found to be more suitably accommodated within the binding pocket of PADs, presumably due to a reduction in steric bulk and the optimal linker length (2-carbon chain) (Figure1).[34,35] These hydantoins were evaluated *in vivo* in the MOG-EAE mouse model of MS demonstrating moderate improvement in clinical scores as well as reduction in CD3+ cells in the treated brain samples in comparison to controls.[33,34] These investigations provided us an insight into the design of non-covalent inhibitors for PAD enzymes, and for their potential applications for the treatment of multiple sclerosis.

Herein we describe the synthesis of a novel class of PAD inhibitors, based on an amino acid backbone, in which similar nitrogen-rich heterocycles were appended via a two-carbon linker to an α-amino acid side chain (Table 1). The structure-activity relationship contained within probed non-covalent binding interactions between the various heterocyclic side chains and active site residues, as well as *N*- and *C*-termini substitutions. *In vitro* PAD inhibition assays were performed to assess their enzyme inhibitory activities, and selectivity towards PAD isozymes. Further, *in vivo* efficacy studies using the MOG EAE mouse model were conducted to demonstrate the potential of this class of non-

covalent inhibitors as new avenues for developing disease modifying therapeutics (DMTs) targeting PAD enzymes.

Table 1. Enzyme inhibition kinetics for non-covalent compounds *h*PAD1, *m*PAD2, and *h*PAD4 and CHO cell toxicity for synthesized non-covalent inhibitors. N/A refers to "data not available".

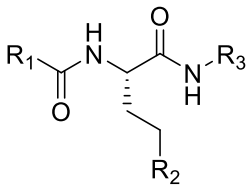

#	R_1	R_2	R_3	K_i (μM)			CHO cells toxicity (IC_{50}, μM)
				***h*PAD1**	***m*PAD2**	***h*PAD4**	
11	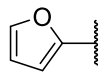	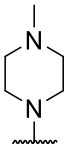	*i*-Pr	N/A	1838 ± 2421	488 ± 47	>2000
12	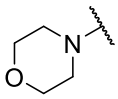	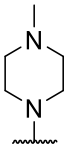	*i*-Pr	>10,000	>10,000	>10,000	>2000
13	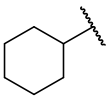	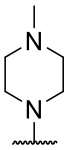	*i*-Pr	N/A	> 10,000	> 10,000	N/A
14	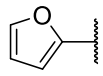	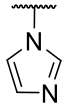	*i*-Pr	964 ± 689	554 ± 93	88 ± 29	546 ±136
15	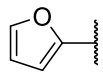	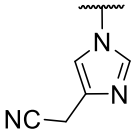	*i*-Pr	353 ± 23	1001 ± 876	591 ± 77	>2000
22	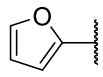	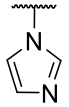	Bn	>10,000	>10,000	>10,000	N/A
23	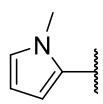	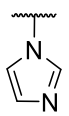	Bn	155 ± 38	60 ± 12	180 ± 12	>2000

28	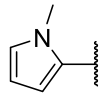	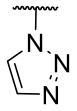	Bn	112 ± 17	71 ± 18	64 ± 28	N/A
29	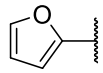	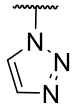	Bn	1,086 ± 499	282 ± 86	2,823 ± 1,804	N/A
30	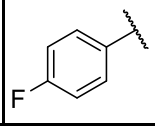	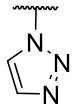	Bn	> 10,000	N/A	N/A	N/A

RESULTS AND DISCUSSION.

Synthesis and Structure-Activity Relationships. A retrosynthetic strategy to afford the chiral target molecules (**11-15**, **22-23** and **29-30**) indicated that enantiopure L-homoserine (**4**) was the ideal backbone for this series of molecules as it set the required linker length to accommodate selected heterocycles at R_2. From here, functional group interconversions and amidations with commercially available reagents could be utilized to scan surface-protein interactions at R_1 and R_3.

Complications with S_N2 substitutions at R_2 owing to a lack of nucleophilicity for the selected *N*-heterocycles necessitated the employment of multiple approaches to synthesize the target compounds. Synthesis of the *N*-methyl piperazine or imidazolyl derivates (**11-15**) is according to Scheme 2. First, protection of the primary alcohol of *L*-homoserine (**4**) with TBDMSCl was followed by amine protection with Fmoc carbamate to afford compound **6** according to published procedures.[36] Treatment of **6** with isopropylamine and HATU afforded intermediate **7** which was subsequently treated with the appropriate acyl chloride to generate the corresponding intermediates **8a-c**. Desilylation followed by mesylation and S_N2 substitution with *N*-methyl piperazine or imidazoles yielded compounds **11-15** (Scheme 2). However, *N*-imidazolyl substitution using the mesylate derivative of **18** did not yield the desired products, **22-23**, due to the formation of elimination byproducts.

Scheme 2. Synthesis of compounds **11-15**.[a]

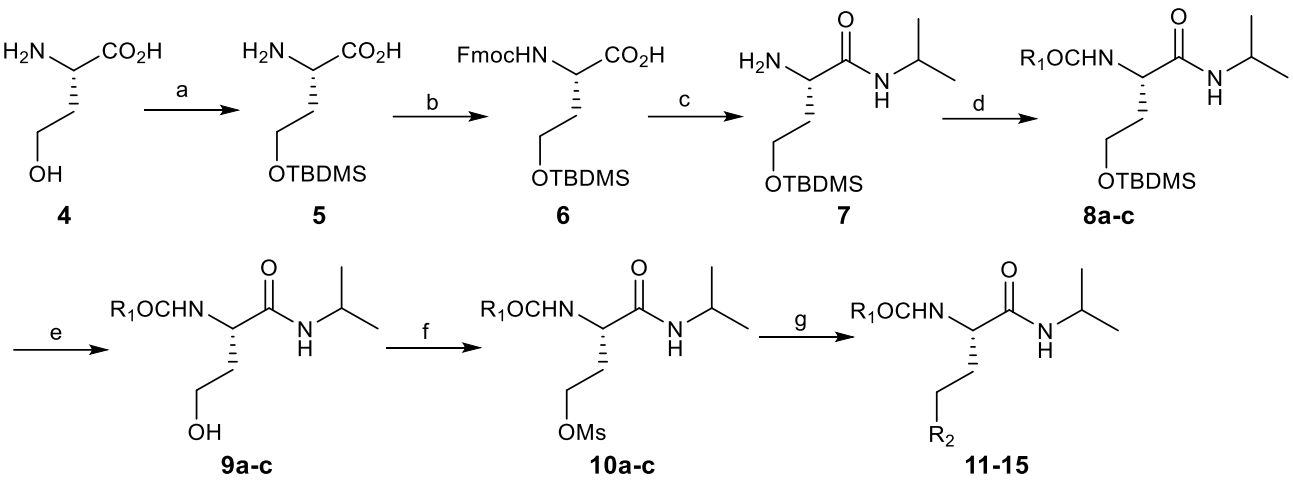

[a]Reagents and conditions: (a) DBU (1.0 eq), TBDMSCl (1.5 eq), anhyd ACN, N_2 atm, rt, 16 h; (b) Fmoc-*O*-Succinate (1.1 eq), Et_3N (1.5 eq), 50:50 ACN: H_2O, rt, 4 h; (c) HATU (1.1 eq), DIPEA (3.0 eq), isopropylamine (10.0 eq), anhyd DMF, N_2 atm, 0 °C→rt, 16 h; (d) R_1COCl (1.0 eq), DIPEA (3.0 eq), anhyd CH_2Cl_2, N_2 atm, 0 °C→rt, 2-5 h; (e) TBAF (1.0 eq), anhyd THF, N_2 atm, 0 °C→rt, 2 hr; (f) MsCl (1.0 eq), DIPEA (3.0 eq), anhyd CH_2Cl_2, N_2 atm, 0 °C, 2 h; (g) R_2-H (1.0 eq), DIPEA (1.5 eq), anhyd DMF, N_2 atm, 0 °C→rt, 16 h.

Thus, a slightly modified procedure was then utilized to afford the target derivatives **22-23** (Scheme 3). Compound **16** was first obtained by amino protection of intermediate **5** with *t*-butoxy carbamate, which exhibited improved stability during the subsequent desilylation step. Coupling of **16** with benzylamine afforded the amide **17**. Desilylation and bromination via Appel reaction[37] afforded **19**. Subsequent substitution with *N*-imidazolyl moiety was optimized when 1*H*-imidazole dissolved in anhyd DMF was first treated with DIPEA (1 eq) and added dropwise to intermediate **19** to afford **20** in good yields. Boc deprotection with TFA afforded **21** which was reacted with appropriate acyl chloride or carboxylic acid to afford compounds **22-23**. The synthesis of compounds **28-30** was carried out via the cyclization of the azide intermediate **24** (Scheme 4), as direct substitutions onto compound **19** with 1*H*,2,3-triazole were unsuccessful. Intermediate **18** was instead converted into azide **24**, followed by 1*H*,2,3-triazole formation with TMS-acetylene in the presence of copper catalyst to yield compound **25**. Desilytation followed by decarbamoylation yielded intermediate **27**, which was coupled with the

appropriate acyl chlorides or carboxylic acids to afford compounds **28-30**.

Scheme 3. Synthesis of *N*-imidazole substituted compounds.[a]

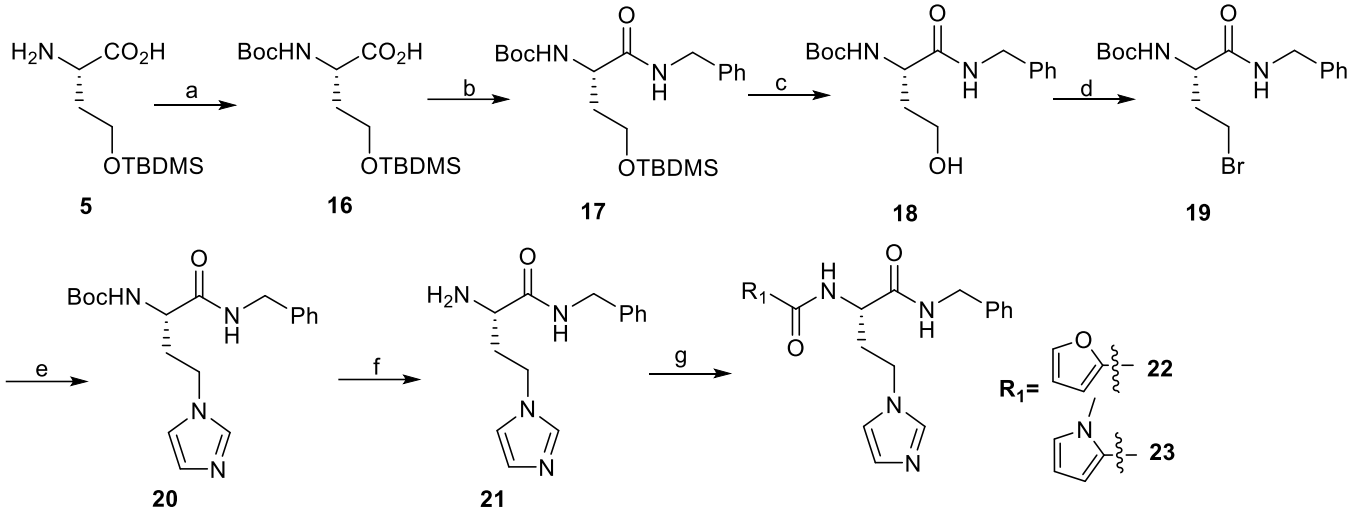

[a]Reagents and conditions: (a) Boc_2O (1.1 eq), Et_3N (1.5 eq), 50:50 ACN:H_2O, rt, 4 hr; (b) HATU (1.10 eq), DIPEA (3.0 eq), benzylamine (1.1 eq), anhyd DMF, N_2 atm, 0 °C→rt, 16 hr; (c) TBAF (1.0 eq), anhyd THF, N_2 atm, 0 °C→rt, 2 hr; (d) CBr_4 (1.5 eq), PPh_3 (1.5 eq), anhyd CH_2Cl_2, N_2 atm, 0 °C→rt, 2.5 hr; (e) imidazole (2.5 eq), DIPEA (1.5 eq), anhyd DMF, N_2 atm, 0°C→rt, 16 hr; (f) 30% TFA, anhyd CH_2Cl_2 , N_2 atm, 0 °C, 45 min; (g) for R_1COCl: DIPEA (3.0 eq), CH_2Cl_2 , N_2 atm, 0 °C, 4 hr; and for R_1COOH: HATU (1.1 eq), DIPEA (3.0 eq), ACN, N_2 atm, 0 °C→rt, 16 hr.

Scheme 4. Synthesis of 1*H*,2,3-triazole substituted non-covalent inhibitors.[a]

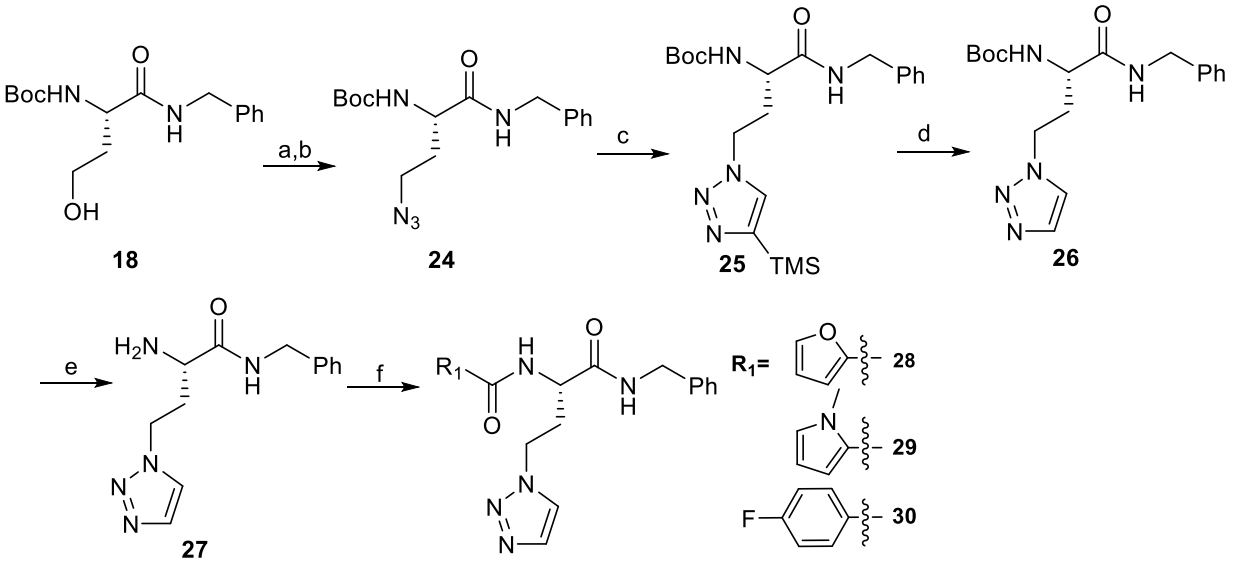

[a]Reagents and conditions: a) MsCl (1.1 eq), DIPEA (3.0 eq), anhyd CH_2Cl_2, N_2 atm, 0 °C, 45 min; b) NaN_3 (4.0 eq), anhyd DMF, N_2 atm, 60 °C, 2.5 h; c) CuI (1.0 eq), TMEDA (1.0 eq), Et_3N (1.0 eq), TMS-acetylene (2.5 eq), anhyd THF, N_2 atm, rt, 18 h; d) TBAF (1.5 eq), anhyd THF, 10% AcOH, N_2 atm, 0 °C→rt, 16 h; e) 30% TFA, anhyd CH_2Cl_2, N_2 atm, 0 °C, 45 min; f) for R_1COCl: DIPEA (3.0 eq), anhyd CH_2Cl_2, N_2 atm, 0 °C, 4 h; for R_1COOH: HATU (1.1 eq), DIPEA (3.0 eq), anhyd ACN, N_2 atm, 0 °C→rt, 16 h.

All synthesized compounds were evaluated for their inhibitory activities against PAD1, PAD2 and PAD4 (Table 1). *N*-Methyl piperazine derivatives (**11-13)**, did not inhibit any of the PAD isozymes. These results were consistent with our previous investigations on hydantoins appended to piperazine motifs via a similar 2-carbon linker,[34] suggesting that the active sites of PADs cannot adequately accommodate non-covalent inhibitors of this size despite the strong basicity of the side chain. Compounds **14**, **15**, **23**, **28** and **29** carrying either imidazoles or a triazole appended to the side chain showed inhibitory activities against at least one PAD isozyme (K_i <400 μM). Among these compounds, **23** and **28** carrying 1-methylpyrroles at R_1 (*N*-terminal) were the most potent compounds with inhibition constants of 60 and 71 μM, respectively, against PAD2 enzyme. Substitution of the pyrrole with a furan at R_1, compounds **22** and **29**, reduced the potency for these compounds (PAD2: K_i >10,000 and 282 μM). Compound **30** did not exhibit any significant inhibition of PAD activities either. Interestingly, furoyl derivative **14** demonstrated good affinity and greater than 6-fold selectivity for PAD4 (K_i = 88 μM) over PAD1 and PAD2; however, further *in vivo* profiling of **14** to investigate the effects of PAD4 inhibiton was contraindicated by a preliminary toxicity screen which showed that compound **14** was moderately cytotoxic to CHO cell lines (IC_{50} = 546 μM). Increasing ring size and introducing ring saturation at R_1 to piperidine resulted in a PAD2 selective reduction in affinity by more than an order of magnitude relative to the 1-methylpyrrole derivatives.

Comparable to the hydantoin series, exemplified by **2** and **3**, PAD enzymes similarily tolerated 5-membered heteroaromatics appended via a 2-carbon linker to the side chain of a core amino acid. Among the peptidomimetic inhibitors, those possessing 1-methylpyrrole subsitutents at R_1 demonstrated the most favorable affinity. The most potent compound in this series, **23** — having demonstrated the highest potentcy and selectivity towards PAD2 — was further investigated *in vivo* to understand its potential in a disease model of MS.

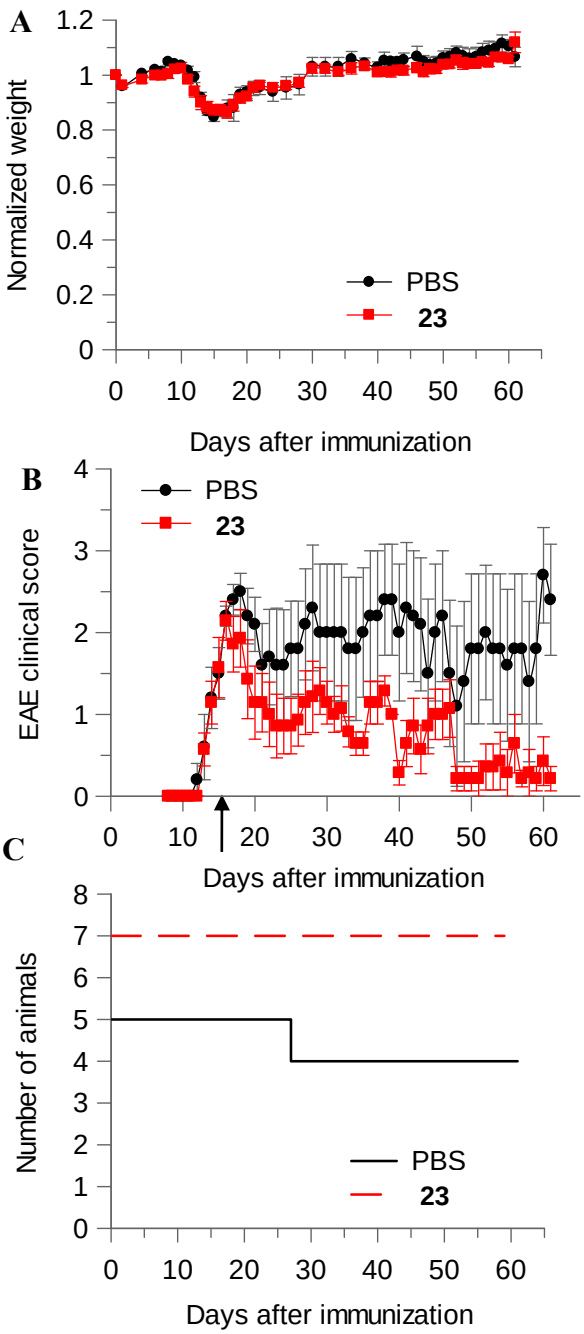

Figure 2. *In vivo* efficacy studies in EAE mice when treated with compound **23**. (A) Normalized weight of EAE mice treated with either PBS or compound **23**, (B) The progression of EAE in C57BL/6 female mice treated with PBS (n=5) or **23** (n=7) — black arrow signals start of treatment, (C) Survival graph showing the mortality rates in PBS-treated and compound **23**-treated mice.

Efficacy Studies. Compound **23** was evaluated in a mouse MOG-EAE model. EAE is an immune-mediated mouse model that mimics the CNS inflammation and lesioning commonly observed in MS

patients, and has been extensively used to evaluate drugs targeting the disease.[38,39] EAE was induced by immunization with myelin oligodendrocyte glycoprotein peptide (MOG_{35-55}). Daily treatment with compound **23** at a dose of 50 mg/kg *i.p.* was initiated once the mice reached a clinical disease score of 2 and was continued for the duration of the study, up to 60 days. EAE clinical scores were recorded for each mouse in the treatment group, and compared to those in the control group, receiving PBS. Body weight was recorded daily for animals in both the treatment and vehicle group as a measure of general toxicity and health, with no difference observed between groups (Figure 2A). Physical disability in the PBS treated mice peaked around the scores of 2-2.5 and remained relatively constant throughout the duration of the study (Figure 2B). In comparison, mice treated with compound **23** showed a significant reduction in EAE clinical scores to the point that nearly complete amelioration of disease symptoms was observed following day 35. The data is also suggestive of a trend towards improved survival rates in the treated *vs* control group (100% vs 80%); although follow up studies with larger sample sizes would be necessary to reach definitive conclusions regarding this outcome measure (Figure 2C).

Both treated and healthy mice of equal age were sacrificed following completion of the study. The brains and spinal cords were collected to analyze for infiltrating T-cells and the status of myelin (Figure 3). We found that by 60 days, there was not as much inflammation in the spinal cord, but we did see some in the brain that differed in extent between the PBS and compound **23**-treated groups. Since the inflammation became more focused in the brain, we analyzed the inflammation in the brain. Thus, these brain sections were subjected to hematoxylin and eosin (H&E) stain, as a general means to detect hypercellularity, as well as Luxol-Fast Blue (LFB) staining to visualize myelin. The number and severity of lesions in the brains of mice treated with PBS were greater than those treated with compound **23**, and the most marked changes were observed in the cerebellum (Figures 3A-C), olfactory tract (Figures 3D-F) and internal capsule (Figures 3G-I). Brain tissue sections, obtained from the mice treated with compound **23**, have the tissue morphology similar to those of healthy mice, and are in complete contrast with those from vehicle treated mice.

Figure 3. Cerebellum of healthy (A) and EAE affected mice (B and C). EAE control animals received PBS and drug treated animals were injected (i.p.) with 50 mg/kg of **23** daily. Yellow arrows point to lessions (perivascular cuffs) formed in the cerebellum of the sick mice. The PBS receiving mice had a higher number of more pronounced lesions as compared to **23** treated mice. Lateral olfactory tract area (Figure D-F) was often observed to be affected by lesions. (E) Shown is a lesion and lymphocytic leptomeningitis in PBS treated mouse. The corresponding areas (indicated by arrows) in healthy and **23** treated mouse are clear. Perivascular leukoencepahlitis, lymphocytic and neutrophilic inflammation along the internal capsule. (G) healthy control, (H) PBS control, (I) compound **23** treated. Magnification 20x. Scale bar indicates 100 µm. Magnification 20x (ImageScope viewer).

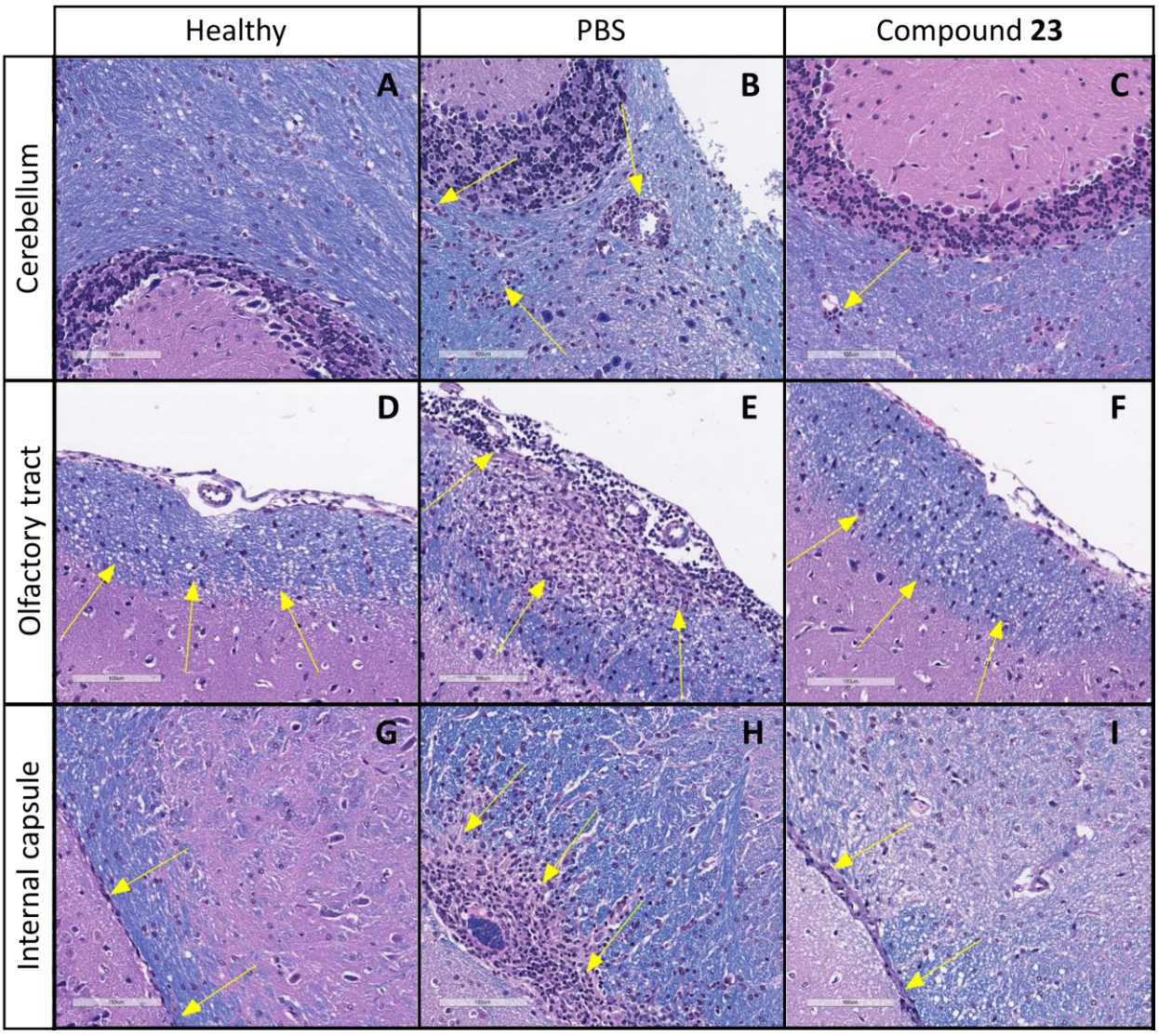

Further immunohistochemical analysis was conducted using anti-CD3 antibodies to investigate the presence of infiltrating T-cells within the mouse brain sections (Figures 4 and 5). The analysis across all stained brain sections suggested that CD3+ T-cell counts were highest in the PBS group, and were

reduced in mice treated with compound **23** (Figure 4).

Corroborating the patterns in the LFB stained brain sections (Figure 3), CD3 markers saw the greatest reduction in the cerebellum (Figure 5A-C) and internal capsule (Figure 5D-F) regions of the brains of the mice treated with **23**. Although this is an animal model of MS, and primarily considered as an inflammation-driven MS model, it is well-characterized that disease pathology such as lesions appearance is localized to cerebellum and internal capsule areas of the brain.[40,41,42]

Figure 4. Immunohistochemistry of EAE affected mice brains. The tissue was probed with CD3+ve antibody to detect T lymphocytes in the CNS of healthy and sick mice. The sick animals were treated with PBS (n = 5) or compound **23** (n =7).

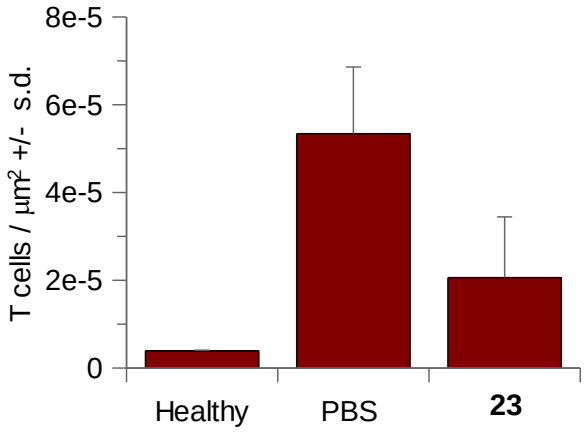

We conducted a single dose pharmacokinetic analysis in healthy mice to determine the levels of compound **23** in the serum and brain (Table 2 and Figure 6). Thus, compound **23** was administered to C57BL/6 female mice *i.p.* (50 mg/kg, single dose), and the serum and brain concentrations were profiled. The maximum concentration (C_{max}) was determined to be 12.0 ± 2.5 µg/mL and 0.17 ± 0.01 µg/mL in the serum and brain, respectively. The C_{max} was observed at 15 min after the administration of **23**, in both serum and brain. The elimination rate constant (k_e) in the serum was 0.02 ± 0.008 min^{-1} and 0.018 ± 0.009 min^{-1} in the brain. The half-life of **23** ($t_{1/2}$) was 34.8 min and 38.5 min in the plasma and brain, respectively. $AUC_{(0\text{-}360)}$ (µg·min/mL) for **23** in the serum and brain were 507.8, and 6.3, respectively. These data indicate the presence of the test compound in the brain with respectable half-life, albeit lower concentrations than those in the serum. Drug metabolism studies and oral

bioavailability, among others are under investigation to understand the behavior of the drug, and its potential fate *in vivo*.

Figure 5. CD3+ staining for T-cells lymphocytes. Shown is the inflammation in cerebellum (A-C) and along the internal capsule (D-F). The inflammation as indicated by the number of infiltrating proinflammatory T cells (yellow arrows) was in general more severe in the PBS receiving mice. The tissue collected from **23**-treated mice showed milder lesions and scattered T cells not clearly associated with any specific lesion. Magnification 20x (ImageScope viewer).

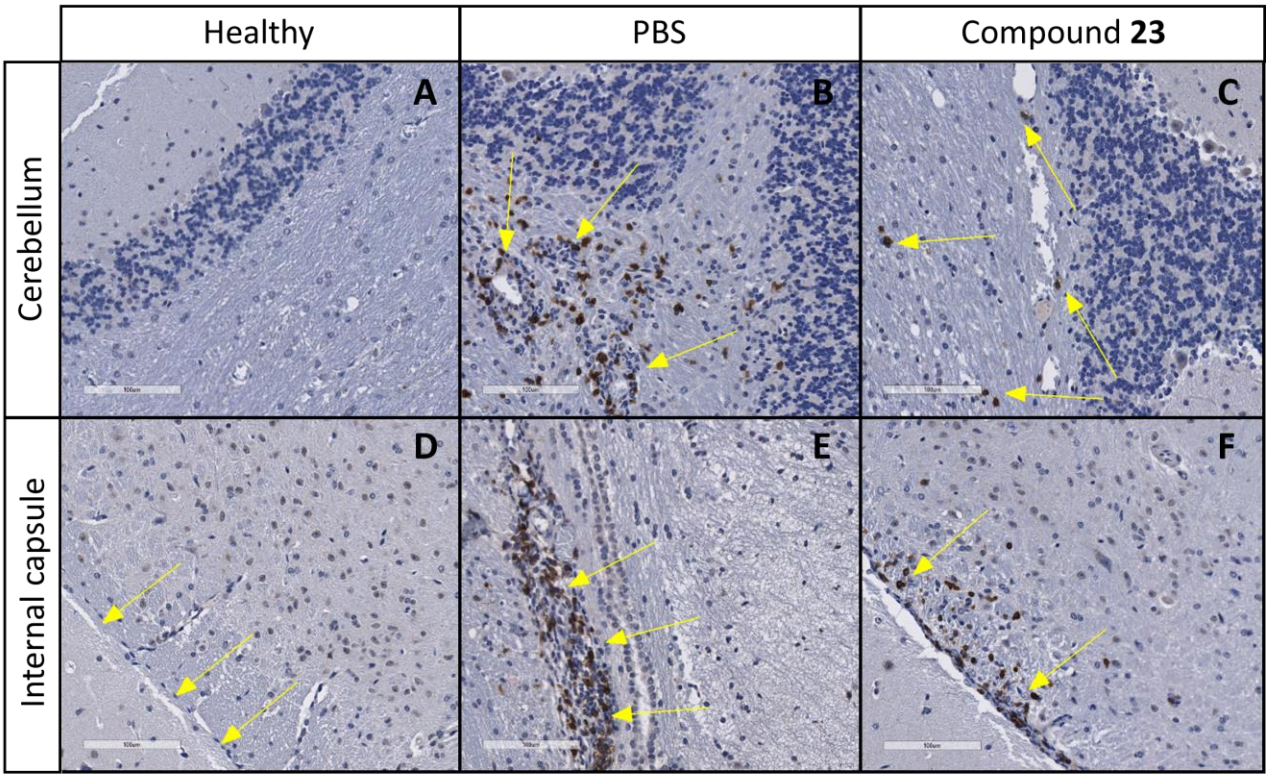

Figure 6. The time-concentration profile for compound **23** in (A) serum and (B) brain of healthy C57BL/6 mice (n=27), measured post-administration.

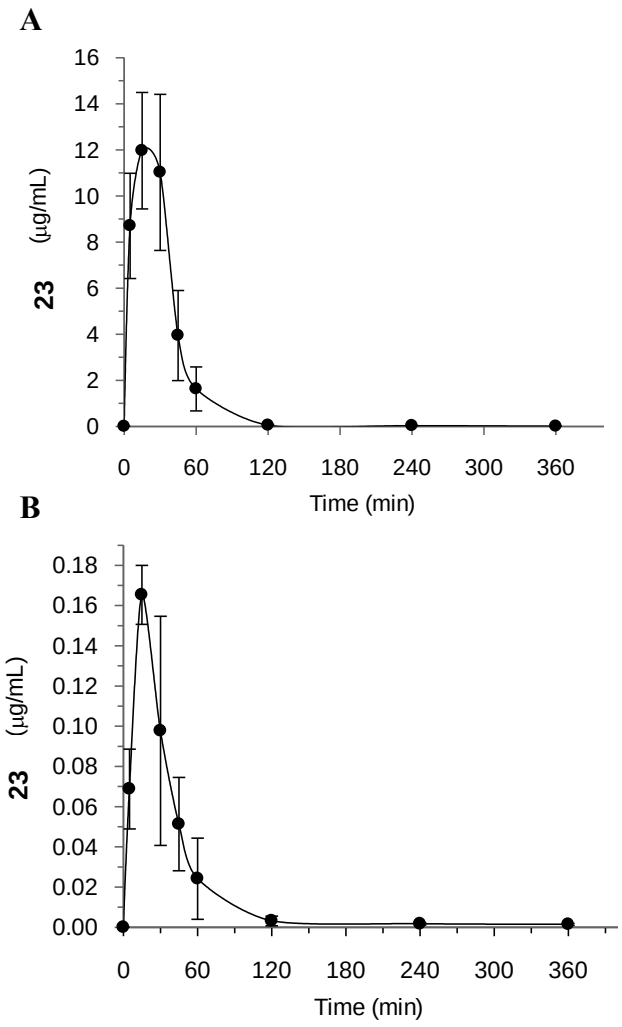

Compound **23**, when compared to compounds **1** and **2** — which are earlier generation non-covalent PAD inhibitors — is more potent *in vivo* (dose of 50 mg/kg *vs* 100 mg/kg). Despite the reduction in dose, the complete recovery of the animals and almost complete suppression of the disease symptoms are noteworthy. Pharmacokinetic studies indicated the presence of compound **23** in the brain, although further studies are required to shed light on the pharmacodynamics and dose-response relationships. The concentration of compound **23** in the brain is low, hence complete abrogation of PAD activities in

the brain may not occur. It is also possible that there may be peripheral effects of compound **23**. However, PAD inhibitors such as **2** exhibit excellent efficacy in cuprizone-mediated demyelinating mouse model of MS that does not involve peripheral inflammation similar to the EAE mouse model.[34] Thus, the efficacy due to **23** is through the moderate inhibition of citrullination in the brain.

Table 2. The pharmacokinetics profile of compound **23** (single dose, 50 mg/kg) in healthy C57BL/6 female mice (n = 27).

Parameter	Serum	Brain
Rate = k_e (min^{-1})	0.02 ± 0.008	0.018 ± 0.009
$t_{1/2}$ (min)	34.8	38.5
C_{max} (μg/mL)	12.0 ± 2.5	0.17 ± 0.01
T_{max} (min)	15	15
$AUC_{(0-360)}$ (μg min /mL)	507.8	6.3

While compound **23** exhibited only minimal selectivity towards PAD2 and may not be among the most potent PAD inhibitors identified to date, its *in vivo* efficacy is impressive. It appears that the inhibition of PAD4, in addition to PAD2, may be necessary for the treatment of complex diseases such as multiple sclerosis, where inflammatory and neurodegenerative components exist. Likewise, its possible that complete abrogation of isozyme specific PAD activities and hence the application of highly-potent and isozyme selective compounds, is not essential nor warranted for treatment. Rather multitargeted PAD inhibitors capable of modestly modulating PAD hyperactivity is sufficient to achieve therapeutic effecicacy. Some evidence can be gleaned from PAD knock-out studies. Raijmakers et al. had shown that PAD2 knockout mice developed EAE despite a lack of PAD2 mediated MBP citrullination, and assumed citrullination did not facilitate a role in EAE initiation.[43] Later, it was confirmed that significant levels of citrullinated MBP were infact present in the PAD2 knockout mice.[44] The citrullination of MBP was due to the upregulated activity but not overexpression of PAD4 in the brain and spinal cord, with levels of PAD4 found to be similar between the PAD2 knockout and wild type mice.[44] In a recent study, Coudane et al also demonstrated that the absence of

PAD2 in PAD2 (-/-) mice did not have a significant affect on protein citrullination following wound induction/inflammation.[45] Thus, the near complete suppression of EAE clinical scores and the reflection of this efficacy in the reversal of brain tissue pathology in the treated animals warrant further investigations into the utility of multi-targeted PAD inhibitors, in particular compound **23** as a DMT for the potential treatment of MS.

Here, we disclosed a novel set of α-amino acid-based designer molecules carrying unique heterocycles, especially compound **23**, as non-covalent inhibitors to PAD enzymes with a potential for optimization as preclinical lead compounds. These findings and the structural core revealed in this work lend themselves to further development of this class of compounds as potential DMTs for MS.

EXPERIMENTAL SECTION.

Chemistry. *General.* All reagents were purchased from Sigma-Aldrich and Bachem chemicals unless otherwise noted. The compounds were purified by column chromatography using silica gel (60 Å, 70-230 mesh) and reverse-phase (C18) silica cartridges. NMR spectra were recorded on a Bruker spectrometer (400 MHz for ^{1}H, 100 MHz for ^{13}C and 376.62 MHz for ^{19}F). Chemical shifts δ are reported in ppm with tetramethylsilane (TMS) as a reference standard for ^{1}H, and trifluoroacetic acid (TFA) as an external reference for ^{19}F, and are reported as *s* (singlet), *brs* (broad singlet), *d* (doublet), *dd* (doublet of doublet), *t* (triplet), *q* (quadruplet), and *m* (multiplet). UV-Vis and fluorescence spectra were recorded on a SpectraMax plate reader (GE Healthcare) in dioxane or PBS as a solvent. LC-MS analyses were conducted using a Waters™ system equipped with a Waters™ 2545 binary gradient module system and Waters™ 3100 mass detector. All compounds evaluated in biological assays were found to be more than 95% pure by two methods of HPLC analysis, and the details are presented in the Supporting Materials.

***O*-(*tert*-Butyldimethylsilyl)-*L*-Homoserine (5)**. A solution of *L*-homoserine, **4** (1 g, 8.4 mmol) and DBU (1.32 mL, 8.8 mmol) in anhyd ACN (20 mL) was treated with *t*-butyldimethysilyl chloride (1.32

g, 8.8 mmol) in ACN (20 mL) at 0 °C. The reaction mixture was stirred at rt for 16 h. after which a white precipitate formed. The suspension was filtered, washed with cold ACN (200 mL), cold H_2O (200 mL) and Et_2O (200 mL), and dried under reduced pressure to afford **5** as a white powder (yield: 1.45 g, 74%). m.p: 148-153 °C. ^{1}H NMR (CD_3OD) δ 3.87 (t, J = 6 Hz, 2H), 3.71-3.68 (m, 1H), 2.21-1.93 (m, 2H), 0.93 (s, 9H), 0.12 (s, 6H). ^{13}C NMR (CD_3OD) δ 61.9, 54.7, 34.4, 26.4, -5.4;.

***N*-((9[*H*]-Fluoren-9-yl) methoxy carbonyl)-*O*-(*tert*-butyldimethylsilyl)-*L*-homoserine (6)**. To a solution of **5** (1.45 g, 6.2 mmol) in 100 mL of 5% $NaHCO_3$ (*w/v*) in 50% ACN/H_2O, Fmoc-*O*-succinimide (2.3 g, 6.8 mmol) was added. The reaction mixture was stirred at rt for 12 h, the solvent was partially removed under reduced pressure, and the remaining suspension was acidified to pH 2.0 with 10% citric acid. Aqueous layer was extracted using EtOAc (3 × 200 mL) and dried over $MgSO_4$. Combined organic layers were concentrated under reduced pressure and the crude was purified by silica gel column chromatography (5-40% EtOAc gradient in hexanes) to afford **6** as a white semi-solid (yield: 2.41 g, 85%). ^{1}H NMR ($CDCl_3$) δ 7.57 (d, J = 7.6 Hz, 2H), 7.60 (t, J = 6 Hz, 2H), 7.39 (t, J = 7.6 Hz, 2H), 7.30 (t, J = 7.2 Hz, 2H), 6.15 (d, J = 7.2 Hz, 2H), 4.21 (t, J = 6.8 Hz, 2H), 3.82 (t, 2H), 2.18-2.05 (m, 2H), 0.91 (s, 9H), 0.09 (s, 6H). ^{13}C NMR ($CDCl_3$) δ 156.4, 143.9, 141.4, 127.8, 127.2, 125.2, 120.1, 67.3, 60.7, 53.1, 47.3, 33.5, 25.9, 18.3, -5.5.

(*S*)-2-Amino-4-*tert*-butyldimethylsilyloxy-*N*-isopropylbutanamide (7). Compound **6** (1.64 g, 3.6 mmol) was dissolved in anhyd DMF (5 mL) to which DIPEA (1.9 mL, 1.8 mmol) and HATU (1.51 g, 3.6 mmol) were added and stirred at 4 °C. Isopropylamine (4.56 mL, 36.0 mmol) was added drop wise to the reaction mixture and was further stirred at 4 °C. Upon completion of the reaction, solvent was evaporated and the crude was dissolved in CH_2Cl_2 (15 mL), washed with H_2O (200 mL), brine (200 mL), and dried ($MgSO_4$). All organic layers were combined and were purified by silica gel column chromatography (30-100% EtOAc gradient in hexanes) to afford **7** as an yellow oil (yield: 390 mg, 40%). ^{1}H NMR ($CDCl_3$) δ 6.68 (m, 1H, NH), 6.15 (m, 1H, NH), 4.10 (m, 1H), 4.03 (septet, 1H), 3.75 (m, 2H), 1.97 (m, 1H), 1.95 (m, 1H), 1.13 (d, J = 6 Hz, 6H), 0.91 (s, 9H), 0.075 (d, J = 4 Hz, 6H). ^{13}C

NMR ($CDCl_3$) δ 170.3, 59.5, 51.1, 40.6, 38.2, 30.7, 25.8, 22.2, 22.1, -5.4.

(*S*)-*N*-(4-*tert*-Butyldimethylsilyloxy-1-isopropylamino-1-oxobutan-2-yl)-furan-2-carboxamide (8a). Compound **7** (360 mg, 1.3 mmol) was dissolved in anhyd CH_2Cl_2 (5 mL) to which DIPEA (762 µL, 4.4 mmol) was added at 0 °C, followed by 2-furoyl carbonyl chloride (215 µL, 2.2 mmol) dropwise and the reaction mixture was stirred at 0 °C for 3 h. Solvent was evaporated, the crude was dissolved in CH_2Cl_2 (30 mL), washed with sat. $NaHCO_3$ solution (200 mL), H_2O (until pH was neutralized), brine (200 mL), and dried ($MgSO_4$). Resulting crude was purified by silica gel column chromatography (0-5% MeOH:CH_2Cl_2) to afford **8a** as a yellow resin (yield: 140 mg, 29%). ^{1}H NMR ($CDCl_3$) δ 7.77 (d, J = 8 Hz, 1H), 7.12 (d, J = 4 Hz, 1H), 6.70 (d, J = 8 Hz, 1H), 6.50 (brs, 1H, NH), 4.73 (m, 1H), 4.09 (septet, 1H), 3.92 (m, 1H), 3.81 (m, 1H), 2.16 (m, 1H), 2.06 (m, 1H), 1.12 (d, J = 4 Hz, 6H), 0.93 (s, 9H), 0.105 (d, J = 4 Hz, 6H). ^{13}C NMR (100 MHz, $CDCl_3$) δ 170.0, 158.3, 147.7, 144.1, 114.6, 112.2, 61.0, 51.7, 41.6, 34.4, 26.0, 22.6, 18.4, -5.3.

(*S*)-*N*-(4-*tert*-Butyldimethylsilyloxy-1-isopropylamino-1-oxobutan-2-yl)morpholine-4-carboxamide (8b). Compound **7** (330 mg, 1.20 mmol) was dissolved in anhyd CH_2Cl_2 (5 mL) and DIPEA (1 mL, 6 mmol) was added at 0 °C. Morpholine carbonyl chloride (210 µL, 1.8 mmol) was added dropwise to the reaction at 0 °C. The reaction was monitored as per the procedure described for compound **8a**. Compound **8b** was obtained as a colorless resin (yield: 245 mg, 53%). ^{1}H NMR ($CDCl_3$) δ 6.71 (brs, 1H, NH), 6.02 (m, 1H, NH), 4.41 (q, 1H), 4.04 (dq, 1H), 3.85 (m, 1H), 3.75 (m, 1H), 3.67 (m, 4H), 3.37 (m, 4H), 1.99 (m, 1H), 1.92 (m, 1H), 1.15 (d, J = 4 Hz, 6H), 0.91 (s, 9H), 0.085 (d, J = 4 Hz, 6H). ^{13}C NMR ($CDCl_3$) δ 171.4, 157.5, 66.5, 61.4, 53.0, 44.5, 44.1, 35.3, 26.1, 22.8, 18.5, -5.1.

(*S*)-*N*-(4-*tert*-Butyldimethylsilyloxy-1-isopropylamino-1-oxobutan-2-yl)-cyclohexane carboxamide (8c). Compound **7** (330 mg, 1.2 mmol) was dissolved in anhyd CH_2Cl_2 (5 mL)and DIPEA (1 mL, 6 mmol) was added at 0 °C. Cyclohexyl carbonyl chloride (240 µL, 1.8 mmol) was added dropwise at 0 °C. The reaction was monitored as per procedure described for **8a** to obtain the target compound. Compound **8c** was obtained as a white solid (yield: 200 mg, 52%). m.p: decomp. at 310 °C; ^{1}H NMR

($CDCl_3$) δ 6.61 (brs, 1H, NH), 5.85 (brs, 1H, NH), 4.40 (q, 1H), 4.05 (dq, 1H), 3.89 (m, 1H), 3.77 (m, 1H), 3.33 (m, 4H), 2.03 (m, 1H), 1.91 (m, 1H), 1.59-1.54 (m, 6H), 1.12 (d, J = 4 Hz, 6H), 0.91 (s, 9H), 0.085 (d, J = 4 Hz, 6H). ^{13}C NMR ($CDCl_3$) δ 171.6, 157.3, 61.4 53.0 47.8 44.8 41.2 34.8 25.9 25.5 24.3, 22.6, 22.5, -5.3.

(*S*)-*N*-(4-Hydroxy-1-isopropylamino-1-oxobutan-2-yl) furan-2-carboxamide (9a). Compound **8a** (140 mg, 380 µmol) was dissolved in 5 mL of anhyd THF and TBAF (165 µL, 570 µmol) was added at 0 °C for 30 min. Reaction solvent was evaporated and resulting crude purified by silica gel column chromatography (0-10% MeOH:CH_2Cl_2) to yield **9a** as a yellow resin (yield: 75 mg, 78%). ^{1}H NMR ($CDCl_3$) δ 7.53 (d, J = 7.2 Hz, 1H), 7.45 (m, 1H, NH), 7.13 (d, 1H), 6.75 (d, J = 7.3 Hz, 1H), 6.51 (m, 1H, NH), 4.75 (m, 1H), 4.08 (septet, 1H), 3.72 (m, 2H), 2.09 (m, 1H), 1.83 (m, 1H), 1.16 (d, J = 4 Hz, 6H).

(*S*)-*N*-(4-Hydroxy-1-isopropylamino-1-oxobutan-2-yl)-morpholine-4-carboxamide (9b). Compound **9b** was synthesized from **8b** (245 mg, 632 µmol) following reaction procedure described for **9a**. Compound **9b** was obtained as a white solid (yield: 103 mg, 60%). m.p: 210 °C decomp. ^{1}H NMR ($CDCl_3$) δ 6.04 (d, 1H, NH), 5.75 (m, 1H, NH), 4.45 (septet, 1H), 4.21(brs, 1H, OH), 4.05 (m, 1H) 3.69 (m, 6H), 3.34 (m, 4H), 1.97 (m, 1H), 1.65 (m, 1H), 1.17 (d, J = 4 Hz, 6H). ^{13}C NMR ($CDCl_3$) δ 171.4, 157.5, 66.5, 61.4, 53.0, 44.5, 44.1, 35.3, 26.1, 22.8, 18.5, -5.1.

(*S*)-*N*-(4-Hydroxy-1-isopropylamino-1-oxobutan-2-yl) cyclohexanecarboxamide (9c). Compound **9c** was synthesized from **8c** (200 mg, 520 µmol) following procedure described for synthesis of **9a**. Compound **9c** was afforded as a white resin (yield: 110 mg, 78%). ^{1}H NMR ($CDCl_3$) δ 6.61 (d, 1H, NH), 5.85 (d, 1H, NH), 4.40 (q, 1H), 4.05 (dq, 1H), 3.89 (m, 1H), 3.77 (m, 1H), 3.33 (m, 4H), 2.03 (m, 1H), 1.91 (m, 1H), 1.59-1.54 (m, 6H), 1.12 (d, J = 4 Hz, 6H). ^{13}C NMR ($CDCl_3$) δ 171.6, 157.3, 61.40, 53.0, 47.8, 44.8, 41.2, 34.9, 25.9, 25.5, 24.3, 22.6.

General procedure for the preparation of the L-*N*-R_1-homoserine-OMs (10a-c). Compound **9a** or **9b** or **9c**was dissolved in approximately 5 mL of anhyd CH_2Cl_2 to which DIPEA (3.0 eq) was added at

0 °C. Methanesulfonyl chloride (2.5 eq) was added dropwise to the reaction mixture at 0 °C with continued stirring, and the reaction was quenched with methanol (5 mL) after 2 hrs. Solvent was evaporated, crude was dissolved in 10 mL of CH_2Cl_2, washed with dilute NH_4Cl solution (150 mL), brine (200 mL), and dried ($MgSO_4$). Solvent was evaporated to obtain the corresponding mesylate, **10a-c**. Intermediates were used immediately for the next reaction without further purification.

(*S*)-*N*-(1-(Isopropylamino)-4-(4-methylpiperazin-1-yl)-1-oxobutan-2-yl)furan-2-carboxamide (11). Compound **10a** (50 mg, 150 µmol) was dissolved in 2 mL of anhyd DMF and stirred at 0 °C. 1-methylpiperazine (18.15 µL, 164 µmol) was added drop wise at 0 °C and reaction was allowed to warm up 60 °C and stir for 2 hr. Upon reaction completion, solvent was removed *in vacuo* and resulting crude was dissolved in CH_2Cl_2 (50 mL) and washed with H_2O (150 mL), brine (150 mL) and dried over $MgSO_4$. Crude was purified by silica gel column chromatography in a gradient of 0-10% MeOH in CH_2Cl_2 to afford **11** as a clear semi-solid (yield: 19 mg, 38%). ^{1}H NMR ($CDCl_3$) δ 7.89 (brs, 1H, NH), 7.49 (d, J = 8 Hz, 1H), 7.16 (d, J = 4 Hz, 1H) 6.78 (m, 1H, NH), 6.52 (dd, J = 8 Hz, J = 4 Hz, 1H) 4.47 (m, 1H), 4.28 (m, 1H), 3.69 (m, 4H), 3.39 (m, 4H), 2.79 (m, 2H), 2.20 (m, 2H), 2.12 (s, 3H), 1.21 (d, J = 4 Hz, 6H); MS (ESI) m/z: $[M + H]^+$ calcd for $C_{17}H_{29}N_4O_3^+$ 337.22, found 337.19.

(*S*)-*N*-(1-(Isopropylamino)-4-(4-methylpiperazin-1-yl)-1-oxobutan-2-yl)morpholine-4-carboxamide (12). Compound **12** was synthesized from **10b** (140 mg, 398 µmol) following reaction protocol described for **11**. Compound **12** was obtained as a clear semi-solid (yield: 56 mg, 40%). ^{1}H NMR ($CDCl_3$) δ 4.68 (m, 1H), 4.06 (septet, 1H), 2.73 (m, 2H), 2.43 (s, 3H), 2.37 (m, 8H), 1.12 (d, J = 4 Hz, 6H); MS (ESI) m/z: $[M + H]^+$ calcd for $C_{17}H_{34}N_5O_3^+$ 356.27, found 356.37.

(*S*)-*N*-(1-(Isopropylamino)-4-(4-methylpiperazin-1-yl)-1-oxobutan-2yl) cyclohexanecarboxamide (13). Compound **13** was synthesized from **10c** (50 mg, 144 µmol) following the procedure described for the synthesis of **11**. Compound **13** was obtained as a white solid (yield: 6 mg, 12%). m.p.: 418-420 °C; ^{1}H NMR ($CDCl_3$) δ 6.13 (d, 1H, NH), 4.54 (m, 1H), 4.19 (m, 1H), 4.125 (q, 2H), 2.85 (m, 1H), 2.17 (m, 1H), 2.14 (s, 3H), 1.91-1.37 (m, 10H), 1.23 (d, J = 4 Hz, 6H); MS (ESI) m/z: $[M + H]^+$ calcd

for $C_{19}H_{37}N_4O_2^+$ 353.29, found 353.31.

(*S*)-*N*-(4-(1[*H*]-Imidazol-1-yl)-1-(isopropylamino)-1-oxobutan-2-yl) furan-2-carboxamide (14). A solution of imidazole (54 mg, 793 µmol) and DIPEA (61 mg, 473 µmol) in anhyd DMF (2 mL) was stirred at rt for 30 min. Compound **10a** (100 mg, 301 µmol) was dissolved in 1 mL of anhyd DMF and added dropwise to the reaction mixture, at 0 °C. Upon completion of the reaction, solvent was evaporated *in vacuo* and the resulting crude was dissolved in EtOAc (50 mL) and washed with H_2O (100 mL), brine (100 mL), and dried over $MgSO_4$. Resulting crude was purified by silica gel column chromatography (30-100% EtOAc gradient in hexanes) to afford **14** as a yellow semi-solid (yield: 25 mg, 27%). ^{1}H NMR (400 MHz, $CDCl_3$) δ 7.89 (s, 1H), 7.70 (s, 1H), 7.49 (d, *J*= 7.2 Hz, 1H),7.19 (d, *J* = 4 Hz, 1H), 7.14 (d, *J*= 7.3 Hz, 1H), 7.03 (d, 1H, NH), 6.78 (m, 1H, NH), 6.52 (dd, *J*= 7.2 Hz, *J*= 7.3 Hz, 1H), 6.15 (d, 1H, NH), 4.59 (m, 1H), 4.11 (m, 2H) 4.08 (m, 1H), 2.41 (m, 1H), 2.21 (m, 1H), 1.18 (d, *J* = 4 Hz, 6H). ^{13}C NMR (100 MHz, $CDCl_3$) δ 171.3, 161.3, 137.8, 133.1, 128.7, 128.1, 126.0, 120.6, 113.3, 111.8, 50.3, 43.2, 38.5, 35.8; MS (ESI) m/z: $[M + H]^+$ calcd for $C_{15}H_{21}N_4O_3^+$ 305.16, found 305.16.

(*S*)-*N*-(4-(4-(Cyanomethyl)-1[*H*]-imidazol-1-yl)-1-(isopropylamino)-1-oxobutan-2-yl)furan-2-carboxamide (15). Compound **15** was synthesized from **10a** (140 mg, 421 µmol) following procedure described for **14**, and the product was obtained as a yellow-brown semi-solid (yield: 35 mg, 24%). ^{1}H NMR (400 MHz, $CDCl_3$) δ 7.55 (s, 1H), 7.17 (d, *J* = 7.2 Hz, 1H), 7.07 (d, 1H, NH), 7.03 (m, *J* = 4 Hz, 1H), 6.54 (dd, *J* = 7.2 Hz, *J* = 4 Hz, 1H), 4.55 (m, 1H), 4.05 (m, 2H), 3.74 (m, 1H), 3.67 (s, 2H), 2.34 (m, 2H), 2.18 (m, 2H), 1.15 (d, *J* = 4 Hz, 6H); MS (ESI) m/z: $[M + H]^+$ calcd for $C_{17}H_{22}N_5O_3^+$ 344.17, found 344.27.

***N*-(*tert*-Butoxycarbonyl)-*O*-(*tert*-butyldimethylsilyl)-*L*-homoserine (16)**. Compound **5** (2.36 g, 10.1 mmol) was dissolved in 50% aqueous acetone (50 mL), triethyl amine (2.1 mL, 15.1 mmol) and Boc-anhydride (2.4 g, 11.0 mmol) were added and the reaction mixture was stirred at rt for 6 h. Solvent was evaporated under reduced pressure, and the aqueous layer was acidified to pH 2.0 with 10% citric acid.

The aqueous layer was extracted with EtOAc (3 x 200 mL) and dried ($MgSO_4$). Compound **16** was obtained as a viscous clear oil (yield: 2.72 g, 81%). ^{1}H NMR ($CDCl_3$) δ 5.92 (d, 1H, NH), 4.33 (q, 1H), 3.81 (m, 2H), 2.07 (m, 2H), 1.441 (s, 9H), 0.910 (s, 9H), 0.08 (d, J = 4 Hz, 6H).

***tert*-Butyl (*S*)-(1-(benzylamino)-4-(*tert*-butyldimethylsilyloxy)-1-oxobutan-2-yl)carbamate (17)**. Compound **16** (2.72 g, 8.16 mmol) was dissolved in anhyd ACN (15 mL) and DIPEA (4.25 mL, 24.4 mmol) and HATU (3.41 g, 8.97 mmol) were added at 4 °C. Benzylamine (980 µL, 8.97 mmol) was then added dropwise to the reaction mixture and continued stirred at 4 °C for 6 h. Reaction solvent was evaporated *in vacuo*, crude was dissolved in EtOAc (15 mL), washed with H_2O (150 mL), brine (150 mL), and dried ($MgSO_4$). Crude was purified by silica gel column chromatography (5-30% EtOAC: hexanes) to afford **17** as a clear oil (yield: 2.29 g, 66%). ^{1}H NMR ($CDCl_3$) δ 7.37 (m, 5H), 7.10 (d, 1H, NH), 6.20 (d, 1H, NH), 4.55 (dd, J = 4 Hz, 2H), 4.41 (m, 1H), 3.85 (m, 2H), 2.12 (m, 2H), 1.52 (s, 9H), 0.99 (s, 9H), 0.15 (d, J = 4 Hz, 6H).

***tert*-Butyl (*S*)-(1-(benzylamino)-4-hydroxy-1-oxobutan-2-yl)carbamate (18).** Compound **17** (1.13 g, 2.67 mmol) was dissolved in anhyd THF (10 mL) and stirred at 0 °C. TBAF (1M solution in THF, 2.67 mL, 2.67 mmol) was added drop wise to reaction mixture and further stirred at 0 °C for 30 min. Solvent was removed and the crude was purified by silica gel column chromatography (10-80% EtOAc: hexanes) to afford **18** as a white solid (yield: 680 mg, 83%).^{1}H NMR ($CDCl_3$) δ 7.59 (d, 1H, NH), 7.30-7.20 (m, 5H), 5.86 (d, 1H, NH), 4.38 (dd, J = 4 Hz, 2H), 4.31 (m, 1H), 3.60 (m, 2H), 1.98-1.69 (m, 2H), 1.40 (s, 9H). m.p.: 330-333 °C.

***tert*-Butyl (*S*)-(1-(benzylamino)-4-bromo-1-oxobutan-2-yl)carbamate (19).** Compound **18** (250 mg, 811 µmol) and carbon tetrabromide (318 mg, 959 µmol) were dissolved anhyd CH_2Cl_2 (10 mL) while stirring at 0 °C and triphenylphosphine (403 mg, 1.54 mmol) dissolved in anhyd CH_2Cl_2 (5 mL) was added dropwise to the reaction mixture over 5 min. The stirring was continued for 4 h, the solvent was evaporated and the crude was purified by silica gel column chromatography (10-40% EtOAc:hexanes) to afford compound **19** as a white powder (yield: 173 mg, 58%). ^{1}H NMR ($CDCl_3$) δ 7.59 (d, 1H, NH),

7.22 (m, 5H), 6.09 (d, 1H, NH), 4.41 (dd, *J* = 4 Hz, 2H), 4.31 (m, 1H), 3.39 (m, 2H), 2.42-2.14 (m, 2H), 1.40 (s, 9H). m.p.: 328-330 °C.

***tert*-Butyl-(*S*)-(1-(benzylamino)-4-(1[*H*]-imidazol-1-yl)-1-oxobutan-2-yl)carbamate (20).** A solution of compound **19** (520 mg, 1.40 mmol) in anhyd DMF (3 mL) was treated with a solution of imidazole (238 mg, 3.50 mmol) and DIPEA (366 µL, 2.10 mmol) in DMF (3 mL) at 0 °C, and the reaction was continued for 4 h. Solvent was then evaporated under reduced pressure, the resulting crude was dissolved in EtOAc (100 mL), washed with H_2O (300 mL), brine (300 mL) and dried ($MgSO_4$). The crude product was purified by silica gel column chromatography (0-10% MeOH:CH_2Cl_2) to yield compound **20** as a yellow resin (yield: 380 mg, 76%). ^{1}H NMR ($CDCl_3$) δ 8.17 (s, 1H), 7.32 (d, *J* = 4 Hz, 1H), 7.21 (m, 5H), 6.87 (d, *J* = 4 Hz, 1H), 5.94 (d, 1H, NH), 4.38 (dd, *J* = 4 Hz, 2H), 4.22 (m, 1H), 3.97 (m, 2H) 2.24-1.99 (m, 2H), 1.43 (s, 9H).

(*S*)-2-Amino-*N*-benzyl-4-(1[*H*]-imidazol-1-yl)butanamide (21). Compound **20** (380 mg, 1.06 mmol) in anhyd CH_2Cl_2 (15 mL) was treated with 30%TFA (2 mL) and stirred at 0 °C for 1 h. Reaction mixture was then treated with toluene (5 mL), concentrated under reduced pressure to yield compound **21** as yellow crystalline solid (yield: 356 mg, quant.). This compound was used as such for the next reaction without further purification.

(*S*)-*N*-(1-(Benzylamino)-4-(1[*H*]-imidazol-1-yl)-1-oxobutan-2-yl) furan-2-carboxamide (22). Compound **21** (95 mg, 368 µmol) was dissolved in 3 mL of anhyd CH_2Cl_2 to which DIPEA (320 µL, 1.84 mmol) was added and stirred at 0 °C. 2-Furoyl chloride (36 µL, 366 µmol) was added dropwise at 0 °C to the reaction mixture and the reaction was stirred at 0 °C for 30 min. The reaction was then allowed to warm up to rt and continued stirring for an additional 12 h. Reaction solvent was evaporated and resulting crude was dissolved in 15 mL of EtOAc and washed with sat. $NaHCO_3$ (200 mL), H_2O (until pH was neutralized), brine (200 mL), and dried over $MgSO_4$. Resulting crude was purified by silica gel column chromatography in a 0-5% MeOH gradient in CH_2Cl_2 to afford **21** as a yellow semi-solid (yield: 25 mg, 19%). ^{1}H NMR ($CDCl_3$) δ 8.41(d, *J* = 4 Hz, 2H), 7.69 (s, 1H), 7.47(s, 1H), 7.28

(m, 5H), 7.09 (d, *J* = 4 Hz, 1H), 6.92 (d, 1H), 6.50 (dd, *J* = 4 Hz, 1H), 5.53 (d, 1H, NH) 4.72 (m, 1H), 4.40 (dd, *J* = 4 Hz, 2H), 3.97 (m, 2H) 2.24-1.99 (m, 2H); MS (ESI) m/z: $[M + H]^+$ calcd for $C_{19}H_{21}N_4O_3^+$ 353.16, found 353.25.

(*S*)-*N*-(1-(Benzylamino)-4-(1[*H*]-imidazol-1-yl)-1-oxobutan-2-yl)-1-methyl-1[*H*]-pyrrole-2-carboxamide (23). *N*-Methylpyrrole-2-carboxylic acid (46 mg, 368 µmol) was dissolved in 2 mL of anhyd DMF to which DIPEA (320 µL, 1.84 mmol) and HATU (139 mg, 366 µmol) were added and stirred at 0 °C for 20 min. Compound **21** (95 mg, 368 µmol) dissolved in anhyd DMF (1 mL) was added to the reaction mixture and stirred for an additional hour at 0 °C, and then stirred for 12 h at rt. Solvent was evaporated and crude was dissolved in EtOAc (50 mL), washed with H_2O (100 mL) and brine (100 mL), and dried over $MgSO_4$. Resulting crude was purified by silica gel column chromatography in a 0-15% MeOH gradient in CH_2Cl_2 to afford **23** as a white semi-solid (yield: 35 mg, 26%). ^{1}H NMR ($CDCl_3$) δ 8.18 (s, 1H), 7.53 (d, *J* = 8 Hz, 1H), 7.35 (s, 1H), 7.34 (d, *J* = 4 Hz, 1H), 7.27 (m, 5H), 7.08 (d, *J* = 4 Hz, 1H), 6.92 (s, 1H), 6.74 (s, 1H), 6.09 (d, 1H, NH), 5.54 (d, 1H), 4.63 (m, 1H), 4.40 (dd, *J* = 4 Hz, 2H), 4.00 (m, 2H), 3.88 (s, 3H), 2.24-1.99 (m, 2H). ^{13}C NMR ($CDCl_3$) δ 179.4, 171.1, 162.2, 138.1, 128.8, 127.7, 127.6, 113.1, 107.7, 50.2, 43.62, 3.91, 34.3; MS (ESI) m/z: $[M + H]^+$ calcd for $C_{20}H_{24}N_5O_2^+$ 366.19, found 366.19.

***tert*-Butyl (*S*)-(4-azido-1-(benzylamino)-1-oxobutan-2-yl)carbamate (24).** A solution of compound **18** (1.75 g, 5.68 mmol) in anhyd CH_2Cl_2 (5 mL) was treated with DIPEA (3 mL, 17.2 mmol) and mesyl chloride (483 µL, 6.24 mmol) at 0 °C and the reaction mixture was stirred at rt for 16 h. Reaction mixture was concentrated under reduced pressure, the crude was dissolved in EtOAc (30 mL), washed with dilute NH_4Cl (150 mL) and brine (150 mL), and dried ($MgSO_4$). Combined organic layers were concentrated and the resulting yellow solid was dissolved in anhyd DMF (5 mL) in a reaction vessel. Sodium azide (1.47 g, 22.6 mmol) was then added to reaction and stirred at 60 °C for 2.5 h under N_2 atmosphere. Reaction was allowed to cool to rt, concentrated under reduced pressure and resulting crude was dissolved in EtOAc (30 mL). The crude was then washed with H_2O (150 mL), brine (150

mL), dried over $MgSO_4$, and purified by silica gel column chromatography (10-60% EtOAc: hexanes) to yield compound **24** as a clear resin (yield: 1.04 g, 55%). ^{1}H NMR ($CDCl_3$) δ 7.32-7.24 (m, 5H), 6.68 (brs, 1H, NH), 5.26 (d, 1H, NH), 4.40 (dd, J = 4 Hz, 2H), 4.21 (septet, 1H), 3.41 (m, 2H), 2.09-2.01 (m, 1H), 1.96-1.92 (m, 1H), 1.42 (s, 9H).

***tert*-Butyl (*S*)-(1-(benzylamino) -1-oxo-4-(4-(trimethylsilyl) -1[*H*]-1,2,3-triazol-1-yl) butan-2-yl) carbamate (25).** To a suspension of CuI (245 mg, 1.29 mmol) in anhyd THF (5 mL), TMEDA (200 µL 1.3 mmol), Et_3N (180 µL, 1.29 mmol) and TMS-acetylene (950 µL, 6.86 mmol) were added and stirred at rt. Compound **24** (860 mg, 2.58 mmol) was dissolved anhyd THF (10 mL) and immediately added to the reaction mixture and allowed to stir at rt for 18 h. Reaction was quenched with H_2O and extracted using EtOAc (60 mL). Organic layer was then washed with brine (150 mL), dried ($MgSO_4$) and concentrated under reduced pressure. Resulting crude was purified by silica gel column chromatography (30-60% EtOAc:hexanes) to afford compound **25** as a colorless resin (yield: 600 mg, 54%). ^{1}H NMR ($CDCl_3$) δ 7.57 (s, 1H), 7.51 (m, 1H, NH), 7.28-7.19 (m, 5H), 5.87 (d, 1H, NH), 4.47 (dd, J = 4 Hz, 2H), 4.39 (m, 2H), 4.30 (septet, 1H), 2.47-2.39 (m, 1H), 2.30-2.25 (m, 1H), 1.40 (s, 9H), 0.29 (s, 9H).

***tert*-Butyl (*S*)-(1-(benzylamino) -1-oxo-4-(1[*H*]-1,2,3-triazol-1-yl) butan-2-yl) carbamate (26).** A solution of compound **25** (700 mg, 1.62 mmol) in anhyd THF (10 mL) and 1M glacial AcOH (1 mL), 1.0 M TBAF in THF (1.62 mL, 1.62 mmol) was added at 0 °C. The reaction was allowed to warm up to rt and was stirred for 16 h. Reaction was concentrated under reduced pressure and the crude was purified by silica gel column chromatography (0-5% MeOH:CH_2Cl_2) to yield compound **26** as a colorless resin (yield: 435 mg, 75%). ^{1}H NMR ($CDCl_3$) δ 7.65 (s, 1H), 7.56 (s, 1H), 7.32-7.26 (m, 5H), 6.74 (brs, 1H, NH), 5.32 (d, 1H, NH), 4.47 (dd, J = 4 Hz, 2H), 4.43 (m, 2H), 4.11 (m, 1H), 2.47-2.2.40 (m, 1H), 2.33-2.26 (m, 1H), 1.42 (s, 9H).

(*S*)-2-Amino-*N*-benzyl-4-(1[*H*]-1, 2,3-triazol-1-yl) butanamide (27). A solution of compound **26** (430 mg, 1.2 mmol) in anhyd CH_2Cl_2 (10 mL) was treated with 30% TFA and stirred at 0 °C for 45

min. Reaction was diluted with toluene (3 mL) and concentrated to afford compound **27** as a yellow resin, which was used for next reaction without further purification (crude yield: 620 mg, quant.).

(*S*)-*N*-(1-(Benzylamino)-1-oxo-4-(1[*H*]-1,2,3-triazol-1-yl)butan-2-yl)-1-methyl-1[*H*]-pyrrole-2-carboxamide (28). *N*-Methylpyrrole-2-carboxylic acid (147 mg, 1.18 mmol) was dissolved in 3 mL of anhyd DMF to which HATU (492 mg, 1.29 mmol) and DIPEA (615 µL, 3.53 mmol) were added, and stirred at 0 °C for 45 min. Compound **27** (305 mg, 1.18 mmol) was dissolved in DMF (2 mL) and added dropwise to the mixture at 0 °C, and the reaction mixture was stirred for 16 h at rt. Solvent was evaporated *in vacuo* and the resulting crude was dissolved in EtOAc (30 mL), washed with H_2O (200 mL), brine (200 mL), and dried over anhyd $MgSO_4$. The combined solvents were concentrated and the crude was purified by silica gel column chromatography (0-10% MeOH gradient in CH_2Cl_2) to yield **28** as a white semi-solid (yield: 120 mg, 28%). ^{1}H NMR ($CDCl_3$) δ 7.97 (s, 1H), 7.76 (d, J = 7 Hz, 1H), 7.63 (s, 1H), 7.47 (d, J = 4 Hz, 1H), 7.29-7.19 (m, 5H), 6.77 (d, J = 7 Hz, 1H, NH), 6.05 (d, J = 4 Hz, 1H), 5.30 (d, 1H, NH), 4.62 (septet, 1H), 4.52 (dd, J = 4 Hz, 2H), 4.40 (m, 2H), 3.86 (s, 3H), 2.91-2.79 (m, 1H), 1.83-1.67 (m, 1H); MS (ESI) m/z: $[M + H]^+$ calcd for $C_{19}H_{23}N_6O_2^+$ 367.19, found 367.29.

(*S*)-*N*-(1-(Benzylamino)-1-oxo-4-(1[*H*]-1,2,3-triazol-1-yl)butan-2-yl)furan-2-carboxamide (29). Compound **27** (305 mg, 1.18 mmol) and DIPEA (615 µL, 3.53 mmol) were dissolved in 7 mL of anhyd CH_2Cl_2 and stirred at 0 °C for 45 min. 2-Furoyl chloride (116 µL, 1.18 mmol) was added to the reaction mixture dropwise at 0 °C and the reaction mixture was stirred for an additional 16 h at rt. Solvent was evaporated and resulting crude was dissolved in 20 mL of EtOAc and washed sat $NaHCO_3$ (200 mL), H_2O (until pH was neutralized), brine (200 mL), and dried over $MgSO_4$. Resulting crude was purified by silica gel column chromatography (0-10% MeOH gradient in CH_2Cl_2) to afford **29** as a light brown semi-solid (yield: 75 mg, 18 %). ^{1}H NMR ($CDCl_3$) δ 7.77 (m, 1H, NH), 7.70 (d, J = 7.2 Hz, 1H), 4.56 (s, 1H), 7.49 (d, J = 4 Hz, 1H), 4.45 (s, 1H), 7.29-7.21 (m, 5H), 7.03 (dd, J =7.2 Hz, J = 4 Hz, 1H), 6.48 (brs, 1H, NH), 4.70 (m, 1H), 4.49 (dd, J = 4 Hz, 2H), 4.45 (m, 2H), 2.38-2.33 (m, 1H), 2.43-2.36 (m, 1H). ^{13}C NMR ($CDCl_3$) δ 170.6, 157.9, 146.9, 143.8, 136.9, 129.2, 128.8, 126.7, 112.1,

111.1, 55.7, 46.8, 43.2, 30.1; MS (ESI) m/z: $[M + H]^+$ calcd for $C_{18}H_{20}N_5O_3^+$ 354.16, found 354.22.

(*S*)-*N*-(1-(Benzylamino)-1-oxo-4-(1[*H*]-1,2,3-triazol-1-yl)butan-2-yl)-4-fluorobenzamide (30). *p*-Fluorobenzoic acid (148 mg, 1 mmol) was dissolved in 5 mL of anhyd DMF to which HATU (403 mg, 1 mmol) and DIPEA (510 µL, 2.892 mmol) were added and stirred at 0 °C for 45 min. Compound **27** (250 mg, 0.96 mmol) was dissolved in 2 mL of DMF and added dropwise to the mixture at 0 °C. Reaction mixture was stirred for an additional 16 h, solvent was evaporated, the resulting crude was dissolved in EtOAc (30 mL), washed with H_2O (200 mL), brine (200 mL), and dried over $MgSO_4$. Resulting crude was purified by silica gel column chromatography in a 0-10% MeOH gradient in CH_2Cl_2 to yield **30** as a white solid (yield: 125 mg, 34%). m.p. 180-185 °C. ^{1}H NMR ($CDCl_3$) δ 7.99 (t, 1H), 7.95 (t, 1H), 7.77 (td, 2H), 7.65 (d, 1H), 7.53 (s, 1H), 7.27-7.19 (m, 5H), 7.01 (td, 2H), 4.79 (septet, 1H), 4.46 (dd, J = 4 Hz, 2H), 4.38 (d, 2H), 2.55-2.48 (m, 1H), 2.45-2.39 (m, 1H). ^{13}C NMR ($CDCl_3$) δ 170.9, 166.7, 163.7, 137.7, 129.7, 128.6, 127.5, 115.7, 115.4, 51.1, 46.9, 43.6, 33.3. ^{19}F NMR ($CDCl_3$) δ -107.14 (s); MS (ESI) m/z: $[M + H]^+$ calcd for $C_{20}H_{21}FN_5O_2^+$ 382.17, found 382.31.

***Enzyme inhibition assays*.** Human PAD1 and PAD4, and mouse PAD2 were purchased from SignalChem (Richmond, BC). Benzoyl arginine ethyl ester (BAEE), DTT, diacetyl monoxime, thiosemicarbazide, and ammonium iron (III) sulfate were purchased from Sigma-Aldrich (Oakville, ON). Tris buffer (100 mM Tris, 100 mM NaCl, 10 mM $CaCl_2$, 5 mM DTT and pH 7.5) was employed as "assay buffer" to conduct the assays. Color reagent was prepared by mixing one volume of reagent A (80 mM diacetyl monoxime, 2 mM thiosemicarbazide) and three volumes of reagent B (17.35 % v/v H_3PO_4, 33.7 % v/v H_2SO_4, and 0.765 mg/mL ammonium iron (III) sulfate). The inhibition studies of *h*PAD1, *h*PAD4, and *m*PAD2 were performed at 37 °C. All test compounds were dissolved in DMSO to prepare the stock solutions and were diluted with the assay buffer. Final concentration of DMSO in all samples for incubation was *ca.* 5%. Control reaction contained no inhibitor and the final substrate concentration was 5 mM in each reaction well. Final concentration of *h*PAD1, *h*PAD4 in the enzyme reaction mixture was 50 nM, and for mPAD2, it was 100 nM. The inhibitors were tested at the final

concentrations of 0.1, 0.5, 1, 2, 5, and 10 mM with each enzyme to obtain the dose-response profile. Various concentrations of the inhibitor were incubated with each PAD isozyme and were incubated at 37 °C for 30 min. Subsequently, substrate solution was added, and the incubation was continued for an additional 30 min. Then the color reagent was added (200 µL/reaction well). Reactions were boiled for 15 min in a water bath, cooled on ice, vortexed and centrifuged. Then, 200 µL-aliquots were transferred to a 96-well plate and the absorbance was recorded at 530 nm. All data was processed using Excel and Grafit 5.0 software. The IC_{50} were derived from the nonlinear fit of the data to the IC_{50} equation:

$$y = \frac{Range}{1 + \left(\frac{x}{IC_{50}}\right)^{s}}$$

where Range is the fitted uninhibited value and s is the slope factor. The K_i values were calculated from the IC_{50} using the Cheng-Prussoff equation:

$$K_i = \frac{IC_{50}}{1 + \left(\frac{[S]}{K_M}\right)}$$

The K_M for *h*PAD1, *m*PAD2 and *h*PAD4 using BAEE as substrate was 0.594, 0.276, and 0.475 mM, respectively.

Mouse efficacy studies. The animal studies were performed according the the protocol reviewed and approved by Animal Care Committee at Toronto General Hospital, University Health Network. The storage, handling and use of Pertussis toxin was approved by the UHN Biosafety Committee and by the Public Health Agency of Canada. The MOG peptide was purchased from Stanford Pan Facility. The Pertussis toxin (PTX) was obtained from LIST Biologicals. Incomplete Freund's adjuvant (IFA) (DIFCO) and *Mycobacterium tuberculosis* H37RA (DIFCO) were purchased from BD Biosciences (Canada).

Seven weeks-old female mice (C57BL/6) were purchased from Jackson Laboratories (NY, USA) and were housed in the Animal Resource Center (UHN, Toronto). Animals living quarters are

maintained under regulated light and temperature conditions. The food and water were available *ad libitum*. Experimental autoimmune encephalomyelitis (EAE) was induced in 8 weeks old mice by immunization with myelin oligodendrocyte glycoprotein (MOG_{33-55}) peptide emulsified in complete Freund's adjuvant (100 μg of MOG per mouse via subcutaneous injection) followed by the intraperitoneal administration of PTX (400 ng per mouse). PTX injection was repeated 48 hours after the initial immunization. Mice were monitored daily for the symptoms of disability characteristic of EAE. The symptoms started to develop 8-14 days after the immunization. Mice were weighted and the disability scores were assigned every day according to the well-established scoring system (Table S2, Supplementary Material). The treatment was initiated when the animals' disability was scored 2 (limp tail and mild paresis of at least one hind limb). The stock solution of hydrochloride salt of compound **23** (10mg/mL) was adjusted to pH 7.5 using 1N NaOH solution, and the final concentration was prepared using PBS. Compound **23** was administered daily via intraperitoneal injection at a dose of 50 mg/kg. Control group of animals received an equal volume of PBS. The collected organs were processed and stained at TCP (Toronto Center for Phenogenomics, Toronto, ON). The brain and spinal cord tissues were stained with Luxol Fast Blue (LFB) and Hematoxylin and Eosin (H&E). The brain tissue sections were also treated/stained with antibodies against PAD2, PAD4, citrulline, and CD3+ve T-cells.

Processed tissue sections were digitalized using brightfield scanner ScanScope XT (Aperio Technologies) at 20x maximum magnification. The images were viewed and analyzed using ImageScope (Aperio Technologies). The quantitative analyses for the brain lesions were performed using Positive Pixel Count Algorithm included in the ImageScope program. The extent of inflammation (darker regions in H&E stained tissue sections) was determined by calculating the ratio of the area affected to the total area of the tissue cross section per specimen. Parameters adopted for image processing are given in Supporting Materials (Table S3). For the tissue section analysis, the inflamed areas were manually selected and the number of positive pixels corresponding to the appropriate stain

was obtained using the Positive Pixel Count algorithm. The total area of the tissue was carefully selected excluding hollow spaces (ventricular systems) and the total area was calculated. The number of stained cells per unit area (μm^2) was calculated by averaging a random selection of areas on the tissue sections and counting for the number of stained cells in each area to arrive at the number of stained cells per unit area..

Pharmacokinetics of compound 23. Pharmacokinetic analysis of **23** was conducted in C57BL/6 female mice (n = 27, 18–22 g in weight). The test compound was dissolved in water after the addition of equimolar concentration of HCl. The pH of the compound solution was increased to 6 using 1 M sodium bicarbonate. The final concentration of the compound was 10 mg/mL The animals received a single 50 mg/kg dose of compound via *i.p.* injection. Blood and brain samples were collected at 0 (pre-dose), 5, 15, 30, 45, 60, 120, 240, and 360 min after the drug administration from 3 mice at each time point. Blood samples were spiked with internal standard, benzophenone (final concentration 4 µg/mL), and centrifuged for 10 min at 5000 rpm to obtain serum. Brain samples were harvested and weighed. After the addition of internal standard (10 µL of 84 µg/mL benzophenone per 200 mg of tissue) and water (100 µL per 100 mg of tissue) the brains were homogenized and centrifuged for 10 min at 10,000 rpm. The supernatant was collected and stored in microcentrifuge tubes. Serum and brain samples were frozen at −80 °C and were lyophilized to dryness. The samples were resuspended in methanol, vortexed and centrifuged (10 min at 10,000 rpm) to obtain clear supernatant. The supernatant was diluted with water (70:30).

The serum and brain samples were analyzed for the presence of **23** on a Waters® ACQUITY UPLC H-Class system equipped with Quaternary Solvent Manager and Sample Manager FTN. The detector was a Waters® MS 3100 mass spectrometer, and the column was an Acquity UPLC® BEH column (2.1 × 50 mm, C_{18}, 1.7 µm) maintained at 40 °C. Sample injection volume was10 µL. The mobile phase consisted of (A) 0.1% formic acid in water and (B) 0.1% formic acid in methanol. The flow rate was 0.2 mL/min. The mobile phase gradient was as follows: 0–0.16 min (30% A / 70% B),

0.16–0.8 min (30% A / 70% B → 2% A / 98 %B), 0.8–1.5 min (2% A / 98% B), 1.5–1.8 min (2% A / 98% B → 30% A / 70% B) and 1.8–3.5 min (30% A / 70% B). Mass spectra from 50 to 500 *m*/*z* and individual masses of **23** (366.19 *m*/*z*) and internal standard (183.22 *m*/*z*) were recorded in the positive mode. The chromatograms were processed using Empower 3 software (Waters®) to obtain area under the curve (AUC), and the concentrations of the analyte were derived from the standard curve.

Acknowledgement. LPK would like to acknowledge the financial support from the Canadian Institutes of Health Research (MOP 126040 and PPP136719), Canada Foundation for Innovation, and Ontario Research Fund.

ASSOCIATED CONTENT.

Supporting Information. This material is available free of charge via the Internet at http://pubs.acs.org. Purity, and mass spectral data for compounds **11**-**15**, **22**-**23**, and **28**-**30**; clinical disability score card and software input parameters for tissue section analyses (PDF). An appendix of molecular formula strings (CSV).

AUTHOR INFORMATION.

Corresponding Author. * Tel. (416) 581-7601, E-mail: lkotra@uhnres.utoronto.ca.

Author Contributions. The manuscript was written through contributions of all authors. All authors have given approval to the final version of the manuscript.

Funding Sources. This research was generously funded by the Canadian Institutes of Health Research (MOP 126040 and PPP136719), Canada Foundation for Innovation, and Ontario Research Fund.

ABBREVIATIONS. ACN, Acetonitrile; AD, Alzheimer's disease; AUC, area under curve; BAEE, benzoyl arginine ethyl ester; Boc, tert-Butyloxycarbonyl; CD4, cluster of differentiation 4; CD3,

cluster of differentiation 3; CHO, chinese hamster ovary; CNS, central nervous system; DBU, 1,8-Diazabicyclo[5.4.0]undec-7-ene; DIPEA, N,N-Diisopropylethylamine; DMF, dimethylforamide; DMSO, dimethyl sulfoxide; DMT, disease modifying therapeutic; DTT, Dithiothreitol; EAE, experimental autoimmune encephalomyelitis; Fmoc, fluorenylmethyloxycarbonyl; H&E, hematoxylin and eosin; HATU, 1-[Bis(dimethylamino)methylene]-1H-1,2,3-triazolo[4,5-b]pyridinium 3-oxid hexafluorophosphate; HPLC, high-performance liquid chromatography; IFA, incomplete Freund's adjuvant; LFB, luxol-fast blue; MBP, myelin basic protein; MOG, myelin oligodendrocyte glycoprotein; MS, multiple sclerosis; MsCl, methanesulfonyl chloride; NET, neutrophil extracellular trap; PAD, protein or peptidylarginine deiminase; PBS, phosphate buffered saline; PTX, pertussis toxin; RA, rheumatoid arthritis; TBAF, tetra-n-butylammonium fluoride; TBDMSCl, tert-Butyldimethylsilyl chloride; TFA, trifluoroacetic acid; THF, tetrahydrofuran; TMS, tetramethylsilane; UPLC, ultra performance liquid chromatography.

REFERENCES

1. Baka, Z.; Gyorgy, B.; Geher, P.; Buzas, E. I.; Falus, A.; Nagy, G. Citrullination under physiological and pathological conditions. *Joint Bone Spine* **2012**, *79*, 431-436.
2. Renato GS, C.; Jos WG van, R.; Guido, J. J.; Ger J Pruijn and Jos MH,Raats. Citrullination: A target for disease intervention in Multiple Sclerosis and other inflammatory diseases? *J. Clin. Cell. Immunol.* **2013**, *4*, 1-8.
3. Vossenaar, E. R.; Robinson, W. H. Citrullination and autoimmune disease: 8th Bertine Koperberg meeting. *Ann. Rheum. Dis.* **2005**, *64*, 1513-1515.
4. Dekan, Z.; Vetter, I.; Daly, N. L.; Craik, D. J.; Lewis, R. J.; Alewood, P. F. Alpha-Conotoxin ImI incorporating stable cystathionine bridges maintains full potency and identical three dimensional structure. *J. Am. Chem. Soc.* **2011**, *133*, 15866-15869.
5. Ishigami, A.; Oshawa, T.; Hiratsuka, M.; Taguchi, H.; Kobayashi, S.; Saito, Y.; Murayama, S.; Asaga, H.; Kimura, N.; Maruyama, N. Abnormal accumulation of citrullinated proteins catalyzed by peptidylarginine deiminase in hippocampal extracts from patients with alzheimer's disease. *J. Neurosci. Res.* **2005**, *80*, 120−128.
6. Moscarello, M. A.; Wood, D. D.; Ackerley, C.; Boulias, C. Myelin in multiple sclerosis is developmentally immature. *J. Clin. Invest.* **1994**, *94*, 146-154.
7. Tu, R.; Grover, H.; Kotra, L. P. Peptidyl arginine deiminase (PADs) and neurodegenerative diseases. *Curr. Med. Chem.* **2016**, *23*, 104-114.
8. Koebel, A.; Curiel Tejeda, E. J.; Tu, R.; Kotra, L. P. Peptidyl arginine deiminase (PAD) inhibitors. In *Advances in Studies on Enzyme Inhibitors as Drugs*; Gupta, S. P., Ed.; Nova Science Publishers: New York, 2016.

9. Kotra, L. P.; Park, J. Therapeutic approaches to MS and other neurodegenerative diseases. In *Comprehensive Medicinal Chemistry*, 3rd ed.; Chackalamannil, S., Rotella, D. P., Ward, S. E., Eds.; Elsevier: Oxford, 2017; Vol. 5, pp. 439-473.

10. Pritzker, L. B.; Moscarello, M. A. A novel microtubule independent effect of paclitaxel: the inhibition of peptidylarginine deiminase from bovine brain. *Biochim. Biophys. Acta* **1998**, *1388,* 154-160.

11. Dreyton, C. J.; Anderson, E. D.; Subramanian, V.; Boger, D. L.; Thompson, P. R. Insights into the mechanism of streptonigrin-induced protein arginine deiminase inactivation. *Bioorg. Med. Chem.* **2014**, *22*, 1362-1369.

12. Causey, C. P.; Jones, J. E.; Slack, J. L.; Kamei, D.; Jones, L. E.; Subramanian, V.; Knuckley, B.; Ebrahimi, P.; Chumanevich, A. A.; Luo, Y.; Hashimoto, H.; Sato, M.; Hofseth, L. J.; Thompson, P. R. The development of N-alpha-(2-carboxyl)benzoyl-N(5) (2-fluoro-1-iminoethyl)-l-ornithine amide (o-F-amidine) and N-alpha-(2 carboxyl)benzoyl-N(5)-(2-chloro-1-iminoethyl)-l-ornithine amide (o-Cl-amidine) as second generation protein arginine deiminase (PAD) inhibitors. *J. Med. Chem.* **2011**, *54*, 6919-6935.

13. Luo, Y.; Knuckley, B.; Lee, Y. H.; Stallcup, M. R.; Thompson, P. R. A fluoroacetamidine-based inactivator of protein arginine deiminase 4: design, synthesis, and in vitro and in vivo evaluation. *J. Am. Chem. Soc.* **2006**, *128*, 1092-1093.

14. Subramanian, V.; Knight, J.S.; Parelkar, S.; Anguish, L.; Coonrod, S.A.; Kaplan, M.J.; Thompson, P. R. Design, synthesis, and biological evaluation of tetrazole analogs of Cl-amidine as protein arginine deiminase inhibitors. *J. Med. Chem.* **2015**, *58*, 1337-1344.

15. Jamali, H.; Khan, H.A.; Stringer, J.R.; Chowdhury, S.; Ellman, J.A. Identification of multiple structurally distinct, nonpeptidic small molecule inhibitors of protein arginine deiminase 3 using a substrate-based fragment method. *J. Am. Chem. Soc.* **2015**, *137*, 3616-3621.

16. Jamali, H.; Khan, H.A.; Tjin, C.C.; Ellman, J.A. Cellular activity of new small molecule protein arginine deiminase 3 (PAD3) inhibitors. *ACS Med. Chem. Lett.* **2016**, *7*, 847-851.

17. Bicker, K.L.; Anguish, L.; Chumanevich, A.A.; Cameron, M.D.; Cui, X.; Witalison, E.; Subramanian, V.; Zhang, X.; Chumanevich, A.P.; Hofseth, L.J.; et al. D-amino acid based protein arginine deiminase inhibitors: Synthesis, pharmacokinetics, and in cellulo efficacy. *ACS Med. Chem. Lett.* **2012**, *3*, 1081-1085.

18. Knight, J.S.; Subramanian, V.; O'Dell, A.A.; Yalavarthi, S.; Zhao, W.; Smith, C.K.; Hodgin, J.B.; Thompson, P.R.; Kaplan, M.J. Peptidylarginine deiminase inhibition disrupts NET formation and protects against kidney, skin and vascular disease in lupus-prone MRL/lpr mice. *Ann. Rheum. Dis.* **2015**, *74*, 2199-2206.

19. Jones, J.E.; Slack, J.L.; Fang, P.; Zhang, X.; Subramanian, V.; Causey, C.P.; Coonrod, S.A.; Guo, M.; Thompson, P.R. Synthesis and screening of a haloacetamidine containing library to identify PAD4 selective inhibitors. *ACS Chem. Biol.* **2012**, *7*, 160-165.

20. Slade, D.J.; Fang, P.; Dreyton, C.J.; Zhang, Y.; Fuhrmann, J.; Rempel, D.; Bax, B.D.; Coonrod, S.A.; Lewis, H.D.; Guo, M.; et al. Protein arginine deiminase 2 binds calcium in an ordered fashion: implications for inhibitor design. *ACS Chem. Biol.* **2015**, *10*, 1043-1053.

21. Lewis, H.D.; Liddle, J.; Coote, J.E.; Atkinson, S.J.; Barker, M.D.; Bax, B.D.; Bicker, K.L.; Bingham, R.P.; Campbell, M.; Chen, Y.H.; et al. Inhibition of PAD4 activity is sufficient to disrupt mouse and human NET formation. *Nat. Chem. Biol.* **2015**, *11*, 189-191.

22. Muth, A.; Subramanian, V.; Beaumont, E.; Nagar, M.; Kerry, P.; McEwan, P.; Srinath, H.; Clancy, K.; Parelkar, S.; Thompson, P.R. Development of a selective inhibitor of protein arginine deiminase 2. *J. Med. Chem.* **2017**, *60*, 3198-3211.

23. Moscarello, M. A.; Lei, H.; Mastronardi, F. G.; Winer, S.; Tsui, H.; Li, Z.; Ackerley, C.; Zhang, L.; Raijmakers, R.; Wood, D. D. Inhibition of peptidyl-arginine deiminases reverses protein-

hypercitrullination and disease in mouse models of multiple sclerosis. *Dis. Model. Mech.* **2013**, *6,* 467-478.

24. Moscarello, M.A.; Pritzker, L.; Mastronardi, F.G.; Wood, D.D. Peptidylarginine deiminase: a candidate factor in demyelinating disease. *J. Neurochem.* **2002**, *81*, 335-343.
25. Moscarello, M.A.; Mastronardi, F.G.; Wood, D.D. The role of citrullinated proteins suggests a novel mechanism in the pathogenesis of multiple sclerosis. *Neurochem. Res.* **2007**, *32*, 251-256.
26. Yang, L.; Tan, D.; Piao, H. Myelin basic protein citrullination in multiple sclerosis: A potential therapeutic target for the pathology. *Neurochem. Res.* **2016**, *41*. 1845-1856.
27. Brady, G.W.; Murthy, N.S.; Fein, D.B.; Wood, D.D.; Moscarello, M.A. The effect of basic myelin protein on multilayer membrane formation. *Biophys. J.* **1981**, *34*, 345-350.
28. Carrillo-Vico, A.; Leech, M.D.; Anderton, S.M. Contribution of myelin autoantigen citrullination to T cell autoaggression in the central nervous system. *J. Immunol.* **2010**, *184*, 2839-2846.
29. Musse, A.A.; Harauz, G. Molecular "negativity" may underlie multiple sclerosis: role of the myelin basic protein family in the pathogenesis of MS. *Int. Rev. Neurobiol.* **2007**, *79*, 149-172
30. Deraos, G.; Chatzantoni, K.; Matsoukas, M.T.; Tselios, T.; Deraos, S.; Katsara, M.; Papathanasopoulos, P.; Vynios, D.; Apostolopoulos, V.; Mouzaki, A.; Matsoukas, J. Citrullination of linear and cyclic altered peptide ligands from myelin basic protein (MBP(87-99)) epitope elicits a Th1 polarized response by T cells isolated from multiple sclerosis patients: implications in triggering disease. *J. Med. Chem.* **2008**, *51*, 7834-7842.
31. Oguz, K.K.; Kurne, A.; Aksu, A.O.; Karabulut, E.; Serdaroglu, A.; Teber, S.; Haspolat, S.; Senbil, N.; Kurul, S.; Anlar, B. Assessment of citrullinated myelin by 1H-MR spectroscopy in early-onset multiple sclerosis. *AJNR Am. J. Neuroradiol.* **2009**, *30*, 716-721.
32. Kidd, B.A.; Ho, P.P.; Sharpe, O.; Zhao, X.; Tomooka, B.H.; Kanter, J.L.; Steinman, L.;

Robinson, W.H. Epitope spreading to citrullinated antigens in mouse models of autoimmune arthritis and demyelination. *Arthritis Res. Ther.* **2008**, *10*, R119.

33. Wei, L.; Wasilewski, E.; Chakka, S. K.; Bello, A. M.; Moscarello, M. A.; Kotra, L. P. Novel inhibitors of protein arginine deiminase with potential activity in multiple sclerosis animal model. *J. Med. Chem.* **2013**, *56*, 1715-1722

34. Sarswat, A.; Wasilewski, E.; Chakka, S. K.; Bello, A. M.; Caprariello, A. V.; Muthuramu, C. M.; Stys, P. K., Dunn, S. E.; Kotra, L. P. Inhibitors of protein arginine deiminases and their efficacy in animal models of multiple sclerosis. *Bioorg. Med. Chem.* **2017**, 25, 2643-2656.

35. Bello, A. M.; Poduch, E.; Wei, L.; Moscarello, M.; Kotra, L. P. Interrogation of the active site of protein arginine deiminase (PAD) using designer probes. *ACS Med. Chem. Lett.* **2013**, *4*, 249-253.

36. Nakamura, T.; Noguchi, T.; Kobayashi, H.; Miyachi, H.; Hashimoto, Y. Mono- and dihydroxylated metabolites of thalidomide: synthesis and TNF-alpha production inhibitory activity. *Chem. Pharm. Bull. (Tokyo)* **2006**, *54*, 1709-1714.

37. Appel, R. Tertiary phosphane/tetrachloromethane, a versatile reagent for chlorination, dehydration, and P—N linkage. *Angew. Chem. Int. Ed. Engl.* **1975**, *14*, 801–811.

38. Procaccini, C.; De Rosa, V.; Pucino, V.; Formisano, L.; Matarese, G. Animal models of multiple sclerosis. *Eur. J. Pharmacol.* **2015**, *759*, 182-191.

39. Kipp, M.; Nyamoya, S.; Hochstrasser, T.; Amor, S. Multiple sclerosis animal models: a clinical and histopathological perspective. *Brain Pathol.* **2017**, *27*, 123-137.

40. Asai, K.; Inagaki, M.; Maegaki, Y.; Yamamoto, T.; Suzuki, I.; Ohta, S. An early-onset case of multiple sclerosis with thalamic lesions on MRI. *Acta Paediatr. Jpn.* **1994**, *36*, 431-434.

41. Charil, A.; Zijdenbos, A.P.; Taylor, J.; Boelman, C.; Worsley, K.J.; Evans, A.C.; Dagher, A. Statistical mapping analysis of lesion location and neurological disability in multiple sclerosis:

application to 452 patient data sets. *NeuroImage* **2003**, *19*, 532-544.

42. Sbardella, E.; Petsas, N.; Tona, F.; Prosperini, L.; Raz, E.; Pace, G.; Pozzilli, C.; Pantano, P. Assessing the correlation between grey and white matter damage with motor and cognitive impairment in multiple sclerosis patients. *PLoS One* **2013**, *8*, e63250.

43. Raijmakers, R.; Vogelzangs, J.; Raats, J.; Panzenbeck, M.; Corby, M.; Jiang, H.; Thibodeau, M.; Haynes, N.; Van Venrooij, W. J.; Pruijn, G. J. M.; Werneburg, B. Experimental autoimmune encephalomyelitis induction in peptidylarginine deiminase 2 knockout mice. *J. Comp. Neurol.* **2006**, *498*, 217-226.

44. Wood, D.D.; Ackerley, C. A.; Brand, B.; Zhang, L.; Raijmakers, R.; Mastronardi, F.G.; Moscarello, M. A. Myelin localization of peptidylartginine deiminases 2 and 4: comparison of PAD2 and 4 activities. *Lab. Invest.* **2008**, *88*, 354-364.

45. Coudane, F.; Mechin, M. C.; Huchenq, A.; Henry, J.; Nachat, R.; Ishigami, A.; Adoue, V.; Sebbag, M.; Serre, G.; Simon, M. Deimination and expression of peptidylarginine deiminases during cutaneous wound healing in mice. *Eur. J. Dermatol.* **2011**, *21*, 376-384.

***Table of Contents* Graphic.**